

Isotopic fractionation of carbon, deuterium and nitrogen: a full chemical study

E. Roueff^{1,2}, J.C. Loison³, and K.M. Hickson³

¹ LERMA, Observatoire de Paris, PSL Research University, CNRS, UMR8112, Place Janssen, 92190 Meudon Cedex, France
e-mail: evelyne.roueff@obspm.fr

² Sorbonne Universités, UPMC Univ. Paris 6

³ ISM, Université de Bordeaux - CNRS, UMR 5255, 351 cours de la Libération, 33405 Talence Cedex, France
e-mail: jean-christophe.loison@u-bordeaux.fr

Received ; accepted

ABSTRACT

Context. The increased sensitivity and high spectral resolution of millimeter telescopes allow the detection of an increasing number of isotopically substituted molecules in the interstellar medium. The $^{14}\text{N}/^{15}\text{N}$ ratio is difficult to measure directly for carbon containing molecules.

Aims. We want to check the underlying hypothesis that the $^{13}\text{C}/^{12}\text{C}$ ratio of nitriles and isonitriles is equal to the elemental value via a chemical time dependent gas phase chemical model.

Methods. We have built a chemical network containing D, ^{13}C and ^{15}N molecular species after a careful check of the possible fractionation reactions at work in the gas phase.

Results. Model results obtained for 2 different physical conditions corresponding respectively to a moderately dense cloud in an early evolutionary stage and a dense depleted pre-stellar core tend to show that ammonia and its singly deuterated form are somewhat enriched in ^{15}N , in agreement with observations. The $^{14}\text{N}/^{15}\text{N}$ ratio in N_2H^+ is found to be close to the elemental value, in contrast to previous models which obtain a significant enrichment, as we found that the fractionation reaction between ^{15}N and N_2H^+ has a barrier in the entrance channel. The large values of the $\text{N}_2\text{H}^+/\text{N}^{15}\text{NH}^+$ and $\text{N}_2\text{H}^+/\text{N}^{15}\text{NH}^+$ ratios derived in L1544 cannot be reproduced in our model. Finally we find that nitriles and isonitriles are in fact significantly depleted in ^{13}C , questioning previous interpretations of observed C^{15}N , HC^{15}N and H^{15}NC abundances from ^{13}C containing isotopologues.

Key words. Astrochemistry – Molecular processes – ISM : molecules – ISM : clouds

1. Introduction

Understanding isotopic abundances on a large scale is a major field of interest which has received a great deal of attention for its application to terrestrial environments (ocean, meteorites), the solar system (planets, comets) and in galactic interstellar space. The variation of isotopic ratios may give us some information about the link between solar system objects and galactic interstellar environments as discussed by Aléon (2010). We principally focus our study on interstellar environments where low temperature conditions may significantly impact the isotopic ratios of the molecular content. Isotopic molecules are detected in a variety of environments and offer an additional tool to determine physical conditions as they usually do not suffer from opacity problems.

Early modeling studies on ^{13}C and ^{18}O isotopic enrichment were performed by Langer et al. (1984) who introduced different isotopic exchange reactions, relying on previous theoretical and experimental studies by Watson et al. 1976; Smith & Adams 1980. Possible effects of selective photodissociation of CO have subsequently been emphasized (Glassgold et al. 1985; Le Bourlot et al. 1993; Visser et al. 2009), which tend to increase the $\text{CO}/^{13}\text{CO}$ ratio. The use of the CN radical as a tracer of $^{12}\text{C}/^{13}\text{C}$ isotopic ratio has been raised by Savage et al. (2002); Milam et al. (2005), who studied the corresponding gradient as a function of the galactic distance. The actual value of the $^{12}\text{C}/^{13}\text{C}$ iso-

topic ratio in the local InterStellar Medium (ISM) is assumed to be 68 (Milam et al. 2005).

The possibility of nitrogen isotopic fractionation in interstellar clouds has been investigated by Terzieva & Herbst (2000) who suggested various ^{15}N isotopic exchange reactions. Rodgers & Charnley (2004, 2008a,b) used these suggested reaction rate constants to predict nitrogen isotopic fractionation in chemical models of dense interstellar molecular cores. They specifically discussed the role of the atomic to molecular nitrogen ratio in the fractionation process and the possible link between nitrogen hydrides and CN containing molecules (nitriles). The corresponding observations are sparse however and difficult as the elemental $^{14}\text{N}/^{15}\text{N}$ ratio is high (441 ± 5), as determined by the recent Genesis solar wind sampling measurement (Marty et al. 2011) and assumed to hold in the local ISM. In addition, the zero point energy (ZPE) differences involved in nitrogen fractionation reactions are small and the predicted corresponding chemical enrichment is moderate. Lucas & Liszt (1998) reported HC^{15}N absorption in diffuse clouds located in front of distant quasars with a $\text{HCN}/\text{HC}^{15}\text{N}$ ratio of 270 ± 27 , close to value reported for the Earth. However, various new observations of isotopic nitrogen containing molecules have been reported, including ^{15}N substituted ammonia and deuterated ammonia (Gerin et al. 2009; Lis et al. 2010), the diazenylium ion (N_2H^+) (Bizzocchi et al. 2010, 2013; Daniel et al. 2013), CN and HCN (Ikeda et al. 2002; Pillai et al. 2007; Adande & Ziurys 2012; Hily-Blant et al. 2013b;

Daniel et al. 2013), HCN and HNC (Wampfler et al. 2014). The strong depletion found in ^{15}N variants of the N_2H^+ isotopologue strongly contradicts model predictions (Gerin et al. 2009), which motivates a reinvestigation of the chemical processes at work. With this in mind, the link between deuterated chemistry and the possible role of ortho/para molecular hydrogen has been studied by Wiström et al. (2012).

We analyse in Section 2 the various possible isotopic exchange reactions that are involved for carbon and nitrogen containing molecules. Indeed, most nitrogen fractionation observational results for CN containing molecules involve only ^{13}C and ^{15}N species so that the measure of the nitrogen isotopic ratio assumes a fixed $^{12}\text{C}/^{13}\text{C}$ fraction. We examine and extend the pioneering study of Terzieva & Herbst (2000) and check for the possible presence of barriers in the entrance channels of isotopic exchange reactions through theoretical calculations. We also update the zero point energy (ZPE) values involved and derive the corresponding exothermicity values. We present our new chemical model in Section 3 and compare with available observations and other models. Our conclusions are presented in Section 5

2. Chemical reactions involving isotopic substitutes of ^{12}C and ^{14}N .

2.1. ^{13}C and ^{15}N exchange reactions

At very low temperatures, isotopic exchange reactions may only occur if no barrier is present between the interacting atoms, ions and molecules or if tunnelling plays an important role. Experimental information is crucial and we constrain the evaluation of rate constants using that information. If no experimental data are available, we apply theoretical methods to determine the presence of a barrier: A first technique uses DFT (Density Functional Theory) calculations (with the hybrid M06-2X functional developed by Zhao & Truhlar (2008) which is well suited for thermochemical calculations, associated to the cc-pVTZ basis set using GAUSSIAN09 software). The alternative is provided by the MRCI+Q method (with the aug-cc-pVTZ basis set). For barrierless cases, we derive the reaction rate constants by using a simple capture theory (Georgievskii & Klippenstein 2005) for both ion-neutral and neutral-neutral reactions. We consider four different families of isotopic exchange reactions:

- *A : direct reactions.* The proton transfer in the $\text{N}_2\text{H}^+ + \text{N}^{15}\text{N} \rightarrow \text{N}^{15}\text{NH}^+ + \text{N}_2$ reaction can serve as an example. In this case and for reactions without a barrier, the reaction rate coefficient of the forward reaction is equal to the capture rate constant multiplied by a probability factor $f(B, M)$, $f(B, M)$ depending on the rotational constant, mass and symmetry values of the reactants and products. In reactions involving ^{15}N and ^{13}C the mass ratio of reactants and products are very close and $f(B, M) \cong \sigma_{\text{entrance channel}}/\sigma_{\text{exit channels}}$ (The symmetry number σ is equal to the number of pathways). The reverse reaction is calculated from the equilibrium constant K , as in Terzieva & Herbst (2000): $K = k_f/k_r = f(B, M) \times \exp(\Delta E/kT)$.
- *B : reactions involving adduct formation leading to direct products without isomerization.* As an example, we refer to $^{15}\text{N}^+ + \text{N}_2 \rightarrow \text{N}^{15}\text{N} + ^{14}\text{N}^+$. We first assume that the high pressure rate constant is equal to the capture rate constant (for reactions without a barrier). We apply statistical theory for the system at thermal equilibrium so that $k_f + k_r = k_{\text{capture}}$. From the equilibrium constant expres-

sion, we then derive $k_f = k_{\text{capture}} \times \frac{f(B, M)}{[f(B, M) + \exp(-\Delta E/kT)]}$ and

$$k_r = k_{\text{capture}} \times \frac{\exp(-\Delta E/kT)}{[f(B, M) + \exp(-\Delta E/kT)]}$$

- *C : reactions involving adduct formation with isomerization pathways.* Such a case holds for $^{13}\text{C} + \text{HCN} \rightarrow ^{12}\text{C} + \text{H}^{13}\text{CN}$. We again assume that the high pressure rate constant is given by capture theory (for reactions without a barrier). The isotopic isomerization reaction competes with the dissociation of the adduct. The rate constant depends on the location of the transition state and statistical calculations are generally required to estimate the isomerization reaction rate constant.
- *D : other reactive exothermic channels exist.* The exchange reaction is discarded generally (the possibility of N atom exchange in the $^{15}\text{N} + \text{CN}$ and in $^{15}\text{N} + \text{C}_2\text{N}$ reactions is discussed).

The knowledge of the exoergicity values ΔE is also a major concern. They are obtained from the differences of the ZPEs between products and reactants. We recall in the Appendix the corresponding expressions and derive their values by using the most recent determinations of spectroscopic constants.

We summarize in Table 1 the different isotopic exchange reactions considered and display the corresponding reaction rate constants. Detailed information is provided in the online material on the theoretical methods used for the different systems. The reactions involving ^{15}N are displayed in the upper part of the Table. We also consider ^{13}C isotopic exchange reactions in the lower part of Table 1. Table 1 shows two main discrepancies compared to previous studies by Terzieva & Herbst (2000) : The exchange reactions between atomic ^{15}N and N_2H^+ , HCNH^+ are found to be unlikely to occur as significant barriers arise in the complex formation step. A similar result is obtained for $^{15}\text{N}^+$ exchange with NO, whereas these reactions had been included in Terzieva & Herbst (2000). The exchange reaction between atomic ^{15}N and CN, which was suggested by Rodgers & Charnley (2008a), is found to be plausible. Additional possibilities of exchange have also been considered such as the reaction between ^{15}N and C_2N . As far as ^{13}C possible fractionation is concerned, we find that CN could be enriched in ^{13}C through the exchange reactions of CN with ^{13}C and $^{13}\text{C}^+$. However, such a mechanism does not hold for HNC as atomic carbon is found to react with HNC (Loison et al. 2014). ^{13}C enrichment of HCN is also found to be unlikely as the calculated transition state lies above the entrance level in the hypothetical isomerization process (C mechanism).

2.2. Ammonia synthesis

Ammonia synthesis proceeds mainly through a chain of reactions starting with $^{14}\text{N}^+$ and H_2 , as the reaction between N and H_3^+ has been shown to be inefficient (Milligan et al. 2000).

2.2.1. The $^{14}\text{N}^+ + \text{H}_2$ reaction and isotopic substitutions

This almost thermoneutral reaction deserves a special mention and has received considerable attention. Le Boulrot (1991) first pointed out the possible role of ortho- H_2 in the interstellar chemistry of ammonia as the energy of its $J=1$ rotational level almost compensates the small endothermicity of the reaction $^{14}\text{N}^+ + \text{H}_2 \rightarrow \text{NH}^+ + \text{H}$. Dislaire et al. (2012) subsequently re-analysed the experimental data (Marquette et al. 1988) and suggested new separate expressions for the reaction rate with p- H_2 and o- H_2 . Similar results were obtained by Zymak et al. (2013), who also emphasized the possible role of the fine structure level of $^{14}\text{N}^+$. We follow the prescription derived by Dislaire et al.

(2012) and extend their analysis to deuterated forms and those including ^{15}N , as displayed in Table 2. In the case of ^{15}N substituted compounds, we have taken into account the (small) additional term due to the change in ZPE. These expressions should be used with caution as in their kinetic expression, we consider that the exponential term represents the enthalpy difference between the products and reactants. The capture rate constant of $^{15}\text{N}^+ + \text{HD}$ reaction is about $(2/3)^{0.5}$ smaller than the rate of the $^{15}\text{N}^+ + \text{H}_2$ reaction, due to the different mass dependences. The formation of $^{15}\text{ND}^+$ is favored at low temperatures.

2.2.2. $\text{NH}_3^+ + \text{H}_2$

The final step of ion-molecule reactions leading to ammonia formation is the reaction between NH_3^+ and H_2 , giving NH_4^+ . Although exothermic, this reaction has a strong temperature dependence, displaying a minimum at $T \sim 100\text{K}$ and a slow increase at lower temperatures (Barlow & Dunn 1987), which is interpreted by the presence of a barrier to complex formation, as discussed in Herbst et al. (1991). At temperatures close to 10K, the reaction is likely to proceed through tunneling which may take place on H atom abstraction. However, the NH_3^+ reaction with D_2 is found to be slower when the temperature decreases as tunneling is not efficient with deuterium. We thus reconsider the isotopic variants of this reaction, as shown in Table 3, where we give the present reaction rates compared to previous values which were derived from Anicich & Huntress (1986). These values are indeed different from those used in our previous studies (Roueff et al. 2005) where we assumed the same rate for the channels resulting from the reactions of NH_3^+ and isotopologues with HD, based on pure statistical considerations. We discuss the resulting modifications in Section 3. Identical reaction rate coefficients are used for the ^{15}N isotopically substituted reactions.

3. Models

3.1. General features

Chemical reactions involving nitrogen atoms and CH, CN and OH have been studied experimentally at low temperatures and shown to be less efficient than previously thought at low temperatures (Daranlot et al. 2012, 2013), which was confirmed by theoretical studies. The corresponding reaction rate constants have been implemented in the KIDA chemical data base (Wakelam et al. 2013) and we have updated our chemical network accordingly. We also include the reactions discussed in Loison et al. (2014) in their study of HCN / HNC chemistry. We explicitly include deuterium, ^{13}C and ^{15}N molecular compounds in our chemical network. The reactions displayed in Table 1, have been included, which allows us to test the hypothesis of a constant $^{12}\text{C}/^{13}\text{C}$ isotopic ratio to derive the $^{14}\text{N}/^{15}\text{N}$ ratio in C^{15}N containing molecules. We take into account the role of the ortho/para ratio of molecular H_2 in the $\text{H}_2\text{D}^+ + \text{H}_2$ and $^{14}\text{N}^+ (^{15}\text{N}^+) + \text{H}_2$ chemical reactions in an approximate way: we do not compute the full ortho/para equilibrium as in the models of Flower et al. 2006; Pagani et al. 2011; Faure et al. 2013 and rather introduce it as a model parameter, which can be varied. Faure et al. (2013) have found a value of 10^{-3} for temperatures below 15K.

Apart from exchange reactions, reactions involving isotopic molecules are assumed to have the same total rate constant as those involving the main isotope except for the reaction of $^{15}\text{N}^+$ with $\text{H}_2/\text{HD}/\text{D}_2$. The various reaction channels are obtained from statistical considerations, in the absence of experimental information. We restrict carbon containing molecules to 3 carbon

atoms, nitrogen containing molecules to 2 nitrogen atoms and consider full deuteration as in our previous studies (Roueff et al. 2005). Within these constraints, the number of species considered in the model is 307 linked through more than 5400 chemical reactions. We consider two different models as displayed in Ta-

Table 4. Model definitions. The $\text{C} / ^{13}\text{C}$ and $\text{N} / ^{15}\text{N}$ ratios are respectively taken as 68 (Milam et al. 2005) and 440 (Marty et al. 2011).

	Model (a)	Model (b)
density n_H (cm^{-3})	2×10^4	2×10^5
Temperature (K)	10	10
cosmic ionization rate per H_2 (s^{-1})	1.3×10^{-17}	1.3×10^{-17}
He / H	0.1	0.1
C / H	4.15×10^{-5}	1.4×10^{-5}
N / H	6.4×10^{-5}	2.1×10^{-5}
O / H	6×10^{-5}	2.0×10^{-5}
S / H	8.0×10^{-8}	8.0×10^{-8}
Fe / H	1.5×10^{-9}	1.5×10^{-9}

ble 4. Model (a) may be considered as a template of TMC1, and assumes a density of hydrogen nuclei $n_H = 2 \times 10^4 \text{ cm}^{-3}$. The elemental abundance of carbon relative to hydrogen nuclei is taken as 4.15×10^{-5} to reproduce the derived relative abundance of CO (Ohishi et al. 1992). We derive the oxygen elemental abundance by imposing a C/O ratio of 0.7 appropriate for TMC1 and take the nitrogen elemental abundance used by Le Gal et al. (2014) in their work on nitrogen chemistry. The elemental abundance of sulfur is not well constrained and we have taken the low metal case value of 8.0×10^{-8} . Model (b) is more representative of a pre stellar core with a density of $2 \times 10^5 \text{ cm}^{-3}$ similar to L134N or Barnard 1 (B1) where the elemental abundances of carbon, oxygen and nitrogen are reduced by a factor of 3 to account for depletion. $T = 10\text{K}$ in both cases and the cosmic ionization rate ζ per H_2 is $1.3 \times 10^{-17} \text{ s}^{-1}$ as in Le Gal et al. (2014).

3.2. Results

We summarize our results obtained with a 10^{-3} value of the o/p ratio of H_2 in Table 5 and give some observational values for comparison. Time dependent effects may be visualized from the values reported at 10^6 years and at steady state for model (a). Steady state is reached after a few 10^7 and 10^6 years respectively for models (a) and (b). As there are fewer ^{15}N enrichment reactions than previously assumed (Terzieva & Herbst 2000) most nitrogen containing species are found to have isotopic abundance ratios close to the solar value ($^{14}\text{N}/^{15}\text{N} = 440$) given by the Genesis mission (Marty et al. 2011).

4. Discussion

We display the time dependence of various isotopic ratios and fractional abundances relative to H_2 and discuss the chemical behavior involved in the fractionation processes for the two reported models. We first consider in Figure 1 the reservoirs of nitrogen, atomic and molecular nitrogen as well as N_2H^+ ions which are chemically linked to N_2 . Atomic nitrogen becomes depleted in ^{15}N after about 10^5 years whereas molecular nitrogen is slightly enriched. These evolution times are also required to build significant amounts of molecular compounds which compare satisfactorily with available observations. The overall dependence of N_2H^+ follows closely that of N_2 as it is formed from $\text{N}_2 + \text{H}_3^+$ reaction, with a slight decoupling between $^{15}\text{NNH}^+$

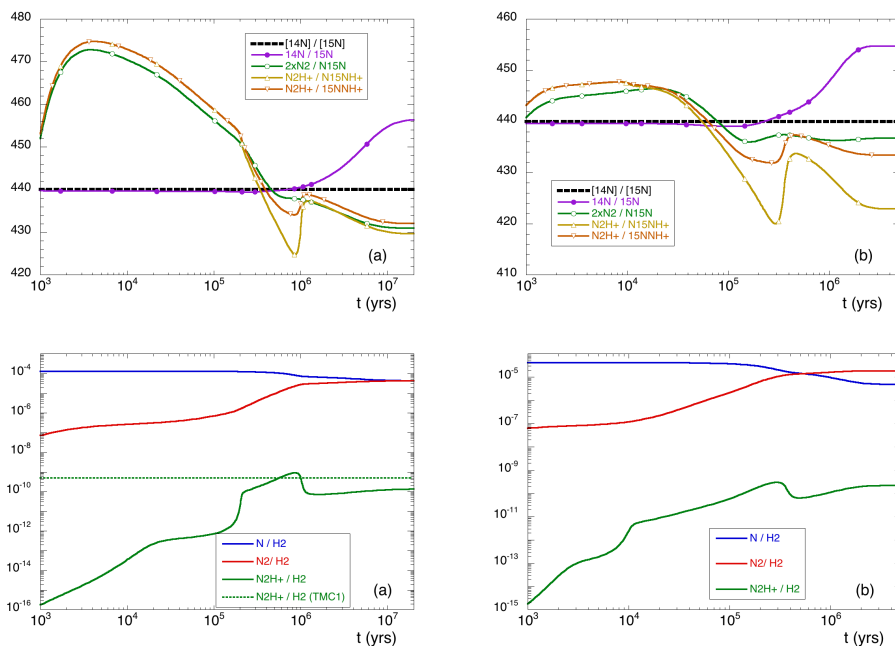


Fig. 1. Upper panel : time dependence of $N / {}^{15}\text{N}$ isotopic ratios in atomic and molecular nitrogen and N_2H^+ ions. (a) and (b) correspond to the models defined in Table 4; the black heavy dotted line represents the elemental $N / {}^{15}\text{N}$. Lower panel : time dependence of the fractional abundances relative to H_2 of N , N_2 and N_2H^+ for models (a) and (b). The value reported for N_2H^+ towards TMC1 (Ohishi et al. 1992) is displayed as a horizontal green dashed line.

and N^{15}NH^+ at long evolution times. We find that the isotopic ratio of the N_2H^+ ions displays an almost constant value close to the solar value after some 10^5 years. They are in good agreement with observations in B1 but disagree by a factor of 2 for L1544. The trend that $\text{N}^{15}\text{NNH}^+$ is less abundant than N^{15}NH^+ is reproduced in our results, as a result of the differences of endothermicity in their reactions with N_2 . We checked that introducing ${}^{15}\text{N}_2$ and species containing two ${}^{15}\text{N}$ atoms had no effect on these ratios. We could not find any gas-phase mechanism able to generate such a large ratio in pre-stellar core conditions. The high isotopic ratio found in L1544 implies an equivalently large ratio for molecular nitrogen, which is in strong contradiction with our findings. These results are markedly different from those derived by Hily-Blant et al. (2013b) who found a moderate ${}^{15}\text{N}$ enrichment as these authors introduced the ${}^{15}\text{N} + \text{N}_2\text{H}^+$ fractionation reaction which we have found not to occur.¹

4.1. Nitrogen hydrides

We display in Figure 2 the time evolution of the isotopic ratios of nitrogen hydrides and of their fractional abundances relative to H_2 . NH_3 and NH_2 have a very similar behavior as they both result from the reaction chain starting with the ${}^{14}\text{N}^+ + \text{H}_2$ reactions. The species NH_2 and NH_3 are found to be enriched in ${}^{15}\text{N}$ due to the ${}^{15}\text{N}^+ + \text{o-H}_2$ reaction which has a slightly smaller (weak) endothermicity, as reported in Table 2, than the corresponding ${}^{14}\text{N}^+ + \text{o-H}_2$ reaction, a difference which slightly favors ${}^{15}\text{NH}^+$ formation. Nevertheless, despite the large uncertainties regarding the rate of the $\text{N}^+ + \text{H}_2$ reaction, our results are in fair agreement with the results of Daniel et al. (2013) for

prestellar core B1. As the $\text{N}^+ + \text{HD} \rightarrow \text{ND}^+ + \text{H}$ reaction has a smaller endothermicity than the $\text{N}^+ + \text{H}_2 \rightarrow \text{NH}^+ + \text{H}$ reaction, the modeled ${}^{14}\text{NH}_2\text{D} / {}^{15}\text{NH}_2\text{D}$ ratio behaves somewhat differently than the ${}^{14}\text{NH}_3 / {}^{15}\text{NH}_3$ ratio. The ratio exhibits large variations around 10^5 years and becomes smaller than that of NH_3 at large times and at steady state. The observed values are compatible with calculations at sufficiently large times. The values of this ratio reported in Gerin et al. (2009) have been found to be too large as a result of assuming a single excitation rotational temperature. The future availability of collisional excitation rates of NH_2D by H_2 (Daniel et al. 2014) may give rise to additional changes. NH does not follow the same trend as NH_2 and NH_3 and is only slightly enriched in ${}^{15}\text{N}$. As discussed by Hily-Blant et al. (2013b), NH is mainly formed from the dissociative recombination (DR) of N_2H^+ , a reaction which has been recently revisited by Vigren et al. (2012) who derive a branching ratio towards NH of 7%. We have checked that this analysis still holds for model (b) even if the reaction of N_2H^+ with CO becomes more efficient. The formation route of NH through NH_2^+ recombination may take over for highly depleted CO .

4.2. Nitriles and isonitriles

Deriving ${}^{15}\text{N}$ isotopic ratios of CN , HCN and HNC from observations is a difficult challenge as the transitions of the main isotopologues are optically thick. Then, most of the reported observational values of the ${}^{14}\text{N} / {}^{15}\text{N}$ molecular ratios are obtained from the ratios of the minor isotopologues ${}^{13}\text{CN} / \text{C}^{15}\text{N}$, $\text{H}^{13}\text{CN} / \text{HC}^{15}\text{N}$ and $\text{HN}^{13}\text{C} / \text{H}^{15}\text{NC}$ which is subsequently multiplied by an assumed $\text{C} / {}^{13}\text{C}$ value, usually taken as 68 (Milam et al. 2005).

¹ These authors also interchanged the endothermicities of the ${}^{15}\text{NNH}^+$ and N^{15}NH^+ reactions with N and N_2 .

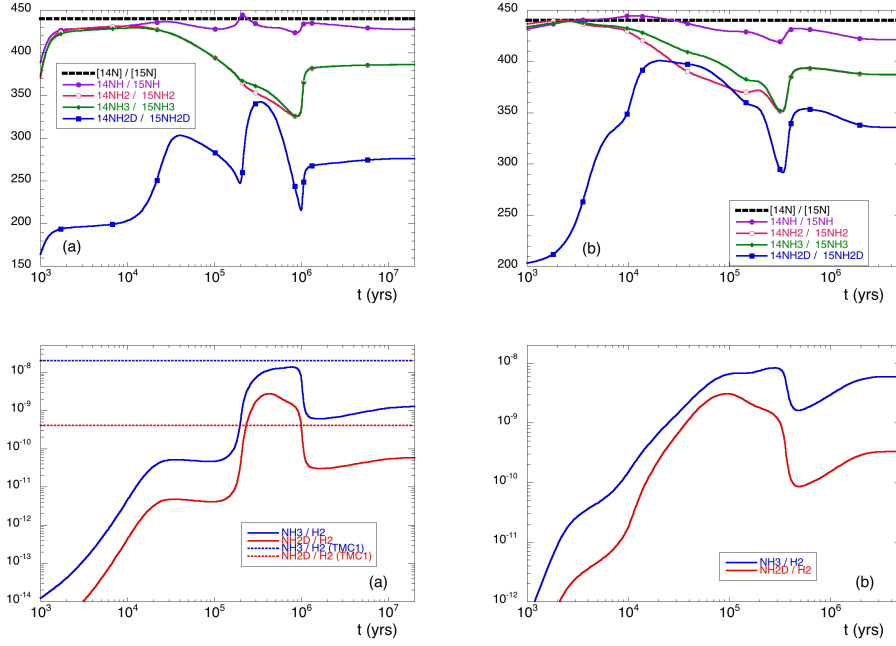


Fig. 2. Upper panel : Time dependence of $\text{N} / ^{15}\text{N}$ isotopic ratios in nitrogen hydrides. (a) and (b) correspond to the models defined in Table 4; The black heavy dotted line represents the elemental $\text{N} / ^{15}\text{N}$. Lower panel : time dependence of the fractional abundances relative to H_2 of NH , NH_2 , NH_3 and NH_2D for models (a) and (b). The values reported for NH_3 (Ohishi et al. 1992) and NH_2D (Tin   et al. 2000) towards TMC1 are displayed as horizontal blue and red dashed lines respectively in the left panel.

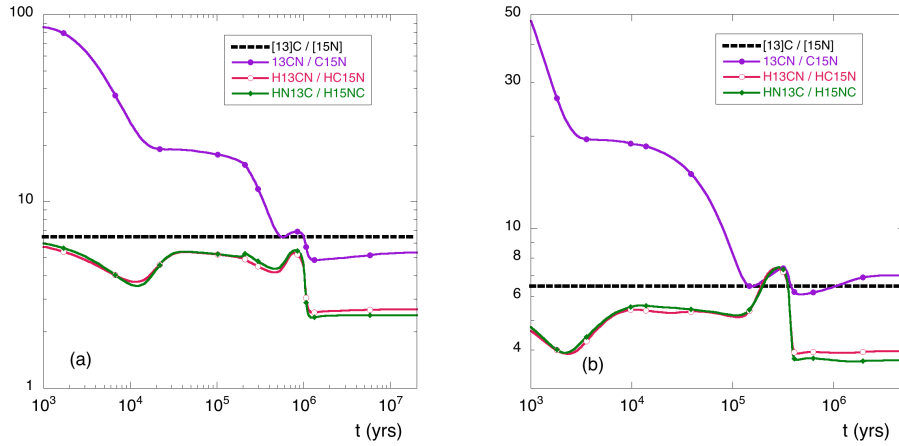


Fig. 3. Time evolution of $^{13}\text{C} / ^{15}\text{N}$ ratios in CN , HCN and HNC for models (a) and (b). The $^{13}\text{C} / ^{15}\text{N}$ elemental ratio is displayed as heavy dotted line.

4.2.1. $^{13}\text{C} / ^{15}\text{N}$ ratios

We test these hypotheses in our models by explicitly introducing fractionation reactions of ^{13}C , as discussed in Section 2. Table 5 shows that the ^{13}C isotopic ratios of CN , HCN and HNC vary both with time and density. Figure 3 displays the $^{13}\text{CN} / ^{15}\text{CN}$, $^{13}\text{HCN} / ^{15}\text{HCN}$ and $^{13}\text{HNC} / ^{15}\text{HNC}$ ratios as a function of time for the two considered models. The deviation from the elemental ratio of 6.48 is significant for HCN , HNC and CN .

4.2.2. ^{13}C chemistry

We now consider the time dependences of the $^{12}\text{C} / ^{13}\text{C}$ isotopic ratios in CN , HCN and HNC species as displayed in Figure 4. The time dependent ratio displays large variations, which is due to the fact that there are various reactions incorporating ^{13}C in the molecules. The elemental value of the ratio (68) is fulfilled in a narrow range around 1 Myr for model (a) and 2×10^5 yrs for model (b) but steady state values are significantly different except for CN . This relatively complex behavior results from the

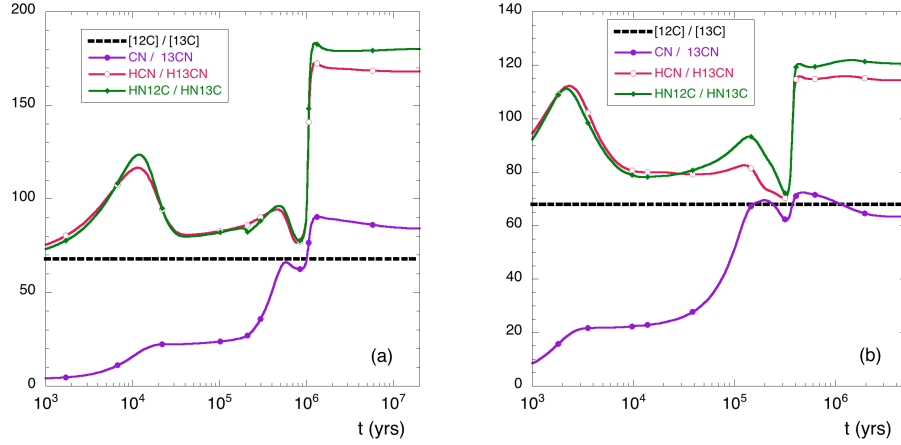


Fig. 4. time dependence of C / ^{13}C isotopic ratios in CN, HCN and HNC. (a) and (b) correspond to the models defined in Table 4

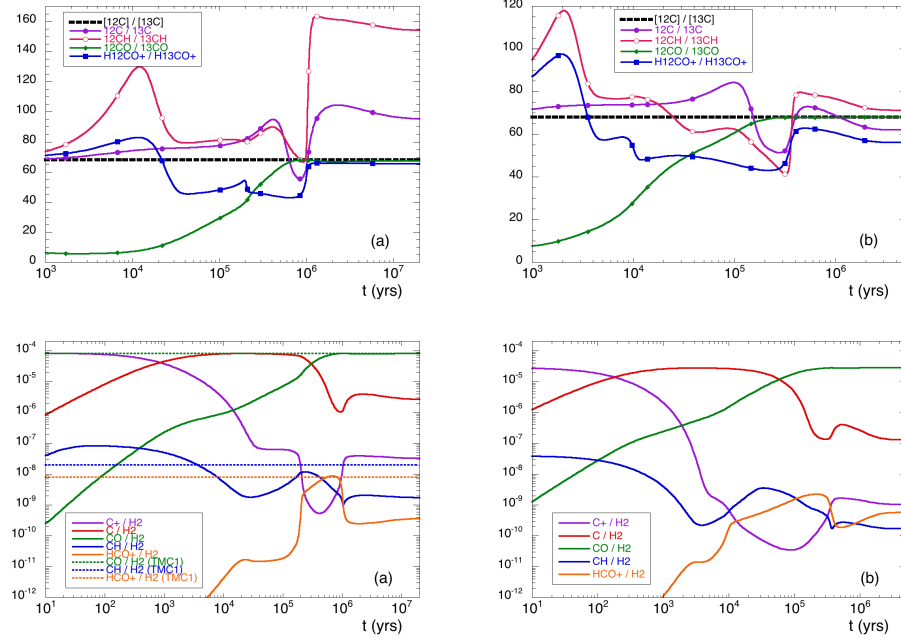


Fig. 5. Upper panel : Time dependence of C / ^{13}C isotopic ratios in C, CH, CO and HCO^+ . The black heavy dotted line represents the elemental $^{12}\text{C} / ^{13}\text{C}$. Lower panel : Time dependence of the fractional abundances relative to H_2 of C, $^{12}\text{C}^+$, CO, CH and HCO^+ , for models (a) and (b). The observational values towards TMC1 (Ohishi et al. 1992) are displayed as horizontal dashed lines with corresponding colors in the left panel. (a) and (b) correspond to the models defined in Table 4

many different reaction channels involved in ^{13}C chemistry. We then also consider other ^{13}C containing species and display the $^{12}\text{C} / ^{13}\text{C}$ ratio in C, CH, CO and HCO^+ in Figure 5 as well as their fractional abundances relative to H_2 . The $^{12}\text{C}/^{13}\text{C}$ isotopic ratios of the various molecules are highly dependent on the evolution time. The transition from gas-phase atomic carbon toward CO controls the ^{13}C enrichment. As long as there is still a relatively high carbon atom concentration in the gas phase, there is enough free ^{13}C to allow strong enrichment of CN through the $^{13}\text{C} + \text{CN}$ reaction. When CO molecules become the reservoir of carbon, even if in that case the ^{13}C concentration is low,

the $^{13}\text{C}^+ + ^{12}\text{CO} \rightarrow ^{12}\text{C}^+ + ^{13}\text{CO}$ reaction still leads to a small ^{13}CO enrichment (Langer & Penzias 1990; Milam et al. 2005). Although this small excess is not measurable in CO, significant amounts of ^{13}C are locked up in CO and most of the other carbon containing species become depleted in ^{13}C , as found for CH and other carbon chains. This effect is seen in Figure 5 for the isotopic ratio of CH in model (a) at steady state where CO is slightly enriched, leading to a significant depletion of ^{13}C in CH. Our results for C and HCO^+ are similar to those of Furuya et al. (2011) who studied the ^{13}C fractionation of multiple carbon chains by explicitly introducing the dependence of the ^{13}C position in the

chain. We see that HCO^+ is marginally enriched in ^{13}C at steady state whereas HCN and HNC are significantly depleted in ^{13}C . We also note that CN and HCO^+ may react via proton transfer to give $\text{CO} + \text{HNC}^+$ and have checked, at the DFT level, the absence of any barrier. The corresponding reaction rate is $2.2 \times 10^{-9} (\frac{T}{300})^{-0.4} \text{ cm}^3 \text{ s}^{-1}$ when using the capture rate theory. This reaction has not been included in any chemical database up to now.

HNC has been shown recently to react with atomic carbon (Loison et al. 2014), which leads to the different steady state isotopic ratios obtained for HCN and HNC . The CN chemistry is then somewhat decoupled from that of HCN and HNC . HCN and HNC are formed at relatively long times via $\text{CN} + \text{H}_3^+ \rightarrow \text{HNC}^+/\text{HCN}^+ + \text{H}_2$, followed immediately by $\text{HNC}^+ + \text{H}_2 \rightarrow \text{HCNH}^+ + \text{H}$ giving back HCN and HNC via DR (Mendes et al. 2012). With the adopted elemental abundances, the main CN destruction reactions are however $\text{O} + \text{CN}$ and $\text{N} + \text{CN}$ so that the $\text{HCNH}^+/\text{HCN}^+/\text{HNC}^+/\text{HCN}/\text{HNC}/\text{CN}$ network is not a closed system in contrast to models including coupled gas-grain chemistry (Loison et al. 2014).

4.2.3. ^{15}N fractionation

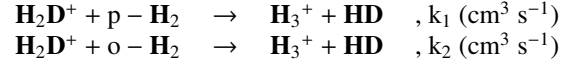
We now display also the $\text{N} / ^{15}\text{N}$ fractionation in nitriles as well as that of NO in Figure 6. The time dependences of the isotopic ratios are markedly different in the two models, except for NO . Whereas CN , HCN and HNC are somewhat enriched in ^{15}N for model (a) both at intermediate times and steady state, the opposite result is obtained in model (b) after 10^5 years. We display as well the time dependences of the fractional abundances of these molecules in Figure 7 in order to better understand the previously described differences observed in the various fractionation ratios.

Our model (a) is intended to be representative of TMC1, a moderately dense cloud in an early evolutionary stage. We see that the various abundances and ratios are very sensitive to the chosen "age", assumed to be the relevant chemical evolution time. Considering a TMC1 age of 1 Myr leads to a reasonable agreement with the sparse observations available, see Table 5. Model (b) is more likely to be representative of a denser evolved molecular cloud such as L134N, L1544, Barnard B1, ... where elemental C, O, N are partially depleted through sticking on grains. Steady state values obtained with significant depletion conditions (Roueff et al. 2005) may be used as corresponding proxies. We see that ammonia isotopologues are satisfactorily accounted for in our model. The agreement between observed and calculated $^{13}\text{C} / ^{15}\text{N}$ ratios is somewhat misleading as the modeled value mainly results from a significant depletion in the ^{13}C species. The ratios involving $\text{N} / ^{15}\text{N}$ are found close to the elemental value in our model (b) at steady state (although NH_2 and NH_3 are somewhat enriched in ^{15}N through the $^{15}\text{N}^+ + \text{H}_2$ reaction as explained in subsection 4.1), which is in agreement with the fact that no significant gas phase fractionation mechanisms have been found. The occurrence of small ratios in B1 observations (Daniel et al. 2013), if real, implies other mechanisms at work. An obvious suggestion lies in the processes involved in adsorption/desorption on grains and possible surface reactions.

4.3. Role of the H_2 ortho to para ratio

We now test the role of the value of the ortho/para ratio of molecular hydrogen (OPR) in the context of ammonia chemistry and fractionation determination. We run two additional models

in the frame of models (a) and (b) by changing the OPR by a factor of 10 both upwards and downwards. The abundances of p- H_2 and o- H_2 are expressed respectively as $n(\text{p-H}_2) = \frac{1}{1+\text{OPR}} n(\text{H}_2)$ and $n(\text{o-H}_2) = \frac{\text{OPR}}{1+\text{OPR}} n(\text{H}_2)$. This ratio is introduced, in addition to the reaction of H_2 with $^{14}\text{N}^+$ ($^{15}\text{N}^+$), in the reverse reaction of the fractionation of H_3^+ , namely the $\text{H}_2\text{D}^+ + \text{H}_2$ reaction which plays a significant role in the deuterium fractionation of various molecules (Pagani et al. 2011) as shown below:



with $k_1 = 2.0 \times 10^{-9} \times \exp(-232/T)$ and $k_2 = 2.0 \times 10^{-9} \times \exp(-61.5/T)$.

Table 7. Dependence of the fractionation ratios on the o/p ratio of H_2 for model (b) at steady state.

	OPR = 10^{-4}	OPR = 10^{-3}	OPR = 10^{-2}
electronic fraction	2.2×10^{-8}	1.7×10^{-8}	1.1×10^{-8}
$\text{N} / ^{15}\text{N}$	457	455	445
$2 \times \text{N}_2 / ^{15}\text{NN}$	436	437	438
$\text{NH} / ^{15}\text{NH}$	425	421	418
NH / ND	9	9	11
$\text{NH}_3 / ^{15}\text{NH}_3$	396	387	416
$\text{NH}_2\text{D} / ^{15}\text{NH}_2\text{D}$	322	336	376
$\text{NH}_3 / \text{NH}_2\text{D}$	11	18	33
$\text{N}_2\text{H}^+ / \text{N}^{15}\text{NH}^+$	425	423	417
$\text{N}_2\text{H}^+ / ^{15}\text{NNH}^+$	434	433	433
$\text{N}_2\text{H}^+ / \text{N}_2\text{D}^+$	8.7	8.6	9.7
$\text{CN} / ^{13}\text{CN}$	65	63	60
$\text{CN} / \text{C}^{15}\text{N}$	449	445	438
$\text{HCN} / \text{H}^{13}\text{CN}$	115	114	107
$\text{HCN} / \text{HC}^{15}\text{N}$	467	453	458
HCN / DCN	25	22	18
$\text{HNC} / \text{HN}^{13}\text{C}$	120	121	118
$\text{HNC} / \text{H}^{15}\text{NC}$	461	446	453
HNC / DNC	19	16	12
$\text{HCO}^+ / \text{H}^{13}\text{CO}^+$	58	56	51
$\text{HCO}^+ / \text{DCO}^+$	8.6	8.4	9.4

Tables 6 and 7 display the fractionation values for the three different assumed values of the OPR for models (a) and (b) and Figures 8 and 9 display the corresponding time evolutions. We see that the curves are almost superposable for times less than 1 Myr for model (a) and less than several 10^5 yrs for model (b). The variations are significative at steady state. We find that the competition between the destruction channels of $^{14}\text{N}^+$ through its reactions with o- H_2 and CO plays a major role. If o- H_2 is the most efficient destruction channel, which occurs typically for $\text{OPR} > 200 \times x_{\text{CO}}$ at 10K, where x_{CO} is the fractional abundance of CO relative to H_2 , formation of NH_4^+ proceeds efficiently. In the opposite case $^{14}\text{N}^+$ is mainly destroyed through reaction with CO to yield CO^+ , leading rapidly to HCO^+ , and NO^+ (which does not react with H_2). As the DR rate coefficients of polyatomic ions increase significantly for larger polyatomic ions (the $\text{NH}_4^+ + \text{e}^-$ reaction is 3 times more rapid than $\text{HCO}^+ + \text{e}^-$ and 20 times more rapid than $\text{H}_3^+ + \text{e}^-$), these two different channels impact the electron abundances and then affect many other species. Moreover, the reaction between NH_3 and H_3^+ leads to $\text{NH}_4^+ + \text{H}_2$. NH_4^+ then reacts mainly with electrons, recycling

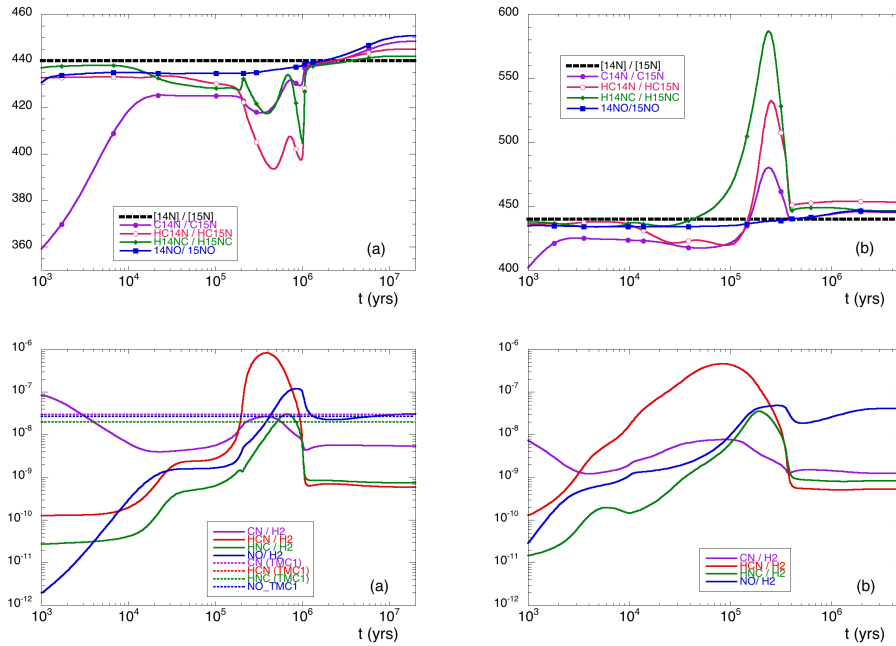


Fig. 6. Time dependence of N / ^{15}N isotopic ratios in CN, HCN, HNC and NO. (a) and (b) correspond to the models defined in Table 4

back to NH_3 which subsequently converts to NH_4^+ , amplifying the electron loss through DR. These effects occur when CO becomes the main carbon reservoir, for sufficiently large evolution times. As a result, the electron fraction is found to decrease when the OPR increases at large evolution times and at steady state. The decreasing electron abundance with increasing OPR values acts to diminish the effect of all DR reactions and as a result to increase the abundances of H_3^+ and H_2D^+ since DR is the main destruction channel in our conditions. The abundance of H_2D^+ is even more enhanced through the $\text{H}_3^+ + \text{HD}$ reaction. Then the abundances of other deuterated molecular ions produced through deuterium transfer reactions of abundant neutrals with H_2D^+ are increased as well, which impacts the subsequent formation of neutral deuterated compounds produced in the DR reactions. Eventually, the HCN/DCN and HNC/DNC ratios are shown to decrease for increasing OPR values. This example demonstrates the complexity of the interplay between the different chemistries.

5. Conclusions

We have built for the first time an isotopically substituted gas phase chemical network including D, ^{13}C and ^{15}N species and included it in a time dependent chemical model. Our model is based on a careful analysis of the possible gas phase mechanisms involved in carbon and nitrogen fractionation by scrutinizing the few available experimental studies and performing DFT and ab-initio quantum calculations on hypothetical reactions to check the possible presence of barriers in the reaction channels. One important result obtained is that the fractionation reaction of ^{15}N with N_2H^+ is unlikely, due to the presence of a barrier, in contrast to the previous hypothesis made by Terzieva & Herbst (2000). As a result, the modeled isotopic ratios involved in the isotopologues of N_2H^+ are found to be very close to the elemental values and are similar to each other, in contradiction with observations towards L1544 (Bizzocchi et al. 2013). The availability of new collisional rate coefficients for the $\text{N}_2\text{H}^+ - \text{H}_2$ sys-

tem (Lique et al. 2015) may however modify these conclusions. We also discarded the $^{15}\text{N} + \text{HCNH}^+$ and $^{15}\text{N} + \text{NO}$ exchange reactions through similar arguments. Tentative reaction rate coefficients are also proposed for carbon fractionation reactions involving $^{13}\text{C}^+$ and ^{13}C with CN and C_2 . Additionally, we have explicitly considered the various isotopologues involved in $\text{N}^+ + \text{H}_2$ reaction, assuming that the energy defect involved in the reactions of $^{14}\text{N}^+$ with para- H_2 is a "real" endothermicity. This leads to a slight decline of the exponential term when $^{15}\text{N}^+$ reacts with H_2 and with HD compared to $^{14}\text{N}^+$. This explains satisfactorily that $^{15}\text{NH}_2\text{D}$ is found to be more enriched in ^{15}N than $^{15}\text{NH}_3$ in the observations. Comparison between observations of nitriles and isonitriles and simulated values is much more questionable, as carbon and nitrogen chemistries are interdependent. Observed isotopic ratios are usually large and suffer from large error bars due to opacity effects in the main isotopologue and difficulties linked to nuclear spin effects. Whereas the various isotopologues follow a similar evolution, the isotopic ratios display significant variations due to slight shifts in the position of the maximum fractional abundances. A reasonable agreement is obtained between the observed $^{13}\text{C} / ^{15}\text{N}$ ratios for most of the species in L134N and Barnard B1 and steady state model values. Our model results show a strong depletion in ^{13}C and a near elemental ratio for $^{14}\text{N} / ^{15}\text{N}$, whereas observations are usually interpreted by assuming an elemental ratio for ^{13}C containing species which leads to the incorrect assumption of ^{15}N enrichment. These considerations are undeniably dependent on the chosen elemental abundances, and in particular to the assumed C/O ratio. We additionally point out a somewhat unexpected effect of the ortho to para ratio of H_2 , which affects significantly the fractional ionization, and consequently the level of deuterium fractionation through the respective orders of magnitude of DR rate coefficients of polyatomic molecular ions. The importance of coupling C, O and N chemistries is emphasized.

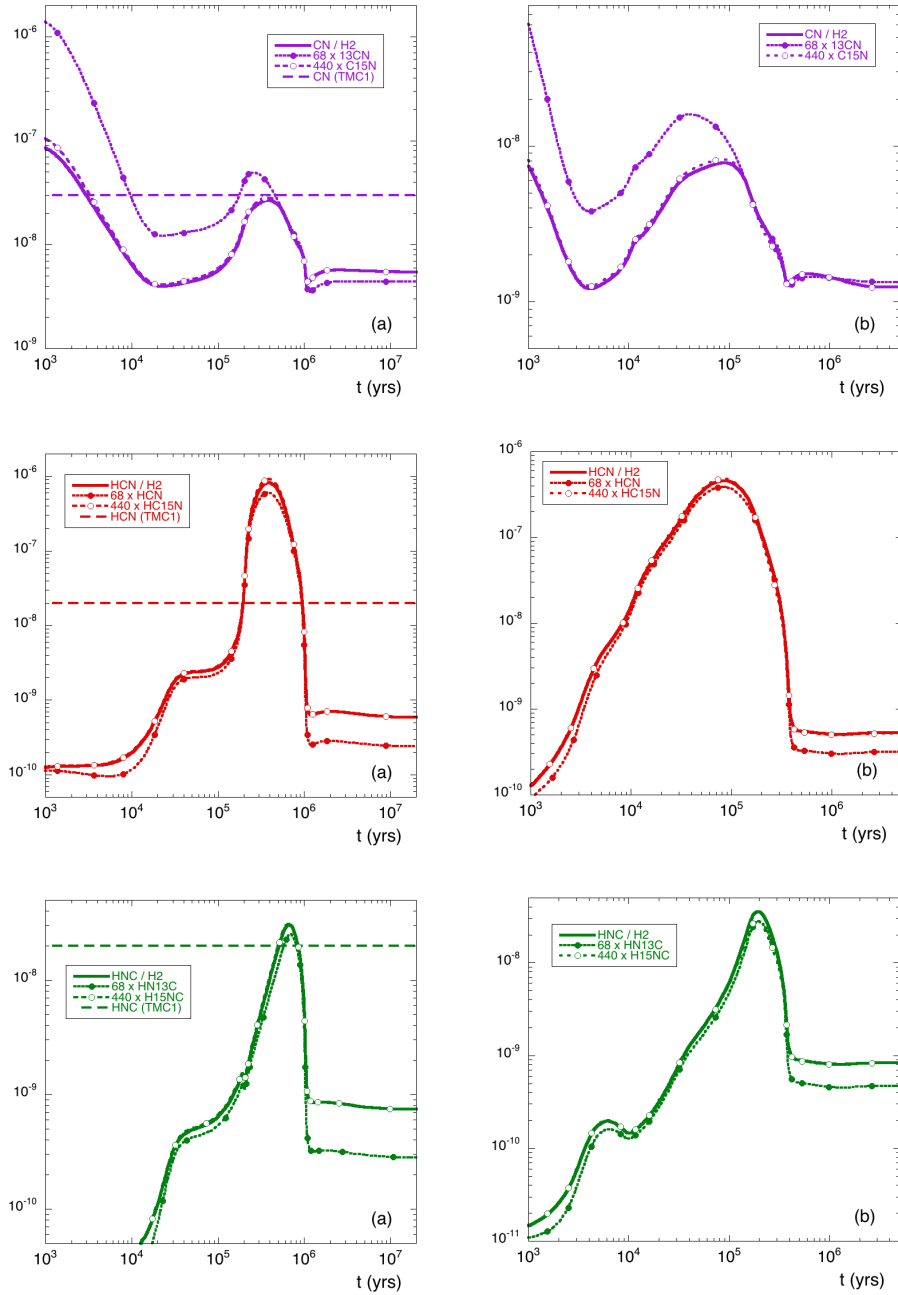


Fig. 7. Time dependence of CN, HCN, HNC and their isotopologues. (a) and (b) correspond to the models defined in Table 4

Acknowledgments

We acknowledge support of PCMI (Programme National de Physique et Chimie du Milieu Interstellaire). This work has been partially funded by the Agence Nationale de la Recherche (ANR) research project IMOLABS (ANR-13-BS05-0008).

References

- Adams, N. G. & Smith, D. 1981, *ApJ*, 247, L123
 Adande, G. R. & Ziurys, L. M. 2012, *ApJ*, 744, 194
 Aléon, J. 2010, *ApJ*, 722, 1342
 Anicich, V. G. & Huntress, Jr., W. T. 1986, *ApJS*, 62, 553
 Anicich, V. G., Huntress, Jr., W. T., & Futrell, J. H. 1977, *Chem. Phys. Lett.*, 47, 488
 Barlow, S. E. & Dunn, G. H. 1987, *International Journal of Mass Spectrometry and Ion Processes*, 80, 227
 Bizzocchi, L., Caselli, P., & Dore, L. 2010, *A&A*, 510, L5
 Bizzocchi, L., Caselli, P., Leonardo, E., & Dore, L. 2013, *A&A*, 555, A109
 Brites, V. & Jutier, L. 2012, *J. Mol. Spectrosc.*, 271, 25
 Colin, R. 1989, *J. Mol. Spectrosc.*, 136, 387
 Colin, R. & Bernath, P. F. 2012, *J. Mol. Spectrosc.*, 273, 30
 Daniel, F., Faure, A., Wiesenfeld, L., et al. 2014, *ArXiv e-prints*
 Daniel, F., Gérin, M., Roueff, E., et al. 2013, *A&A*, 560, A3
 Danielak, J., Kepa, R., & Zachwieja, M. 1997, *Journal of Physics B Atomic Molecular Physics*, 30, 4889
 Daranlot, J., Hincelin, U., Bergeat, A., et al. 2012, *Proceedings of the National Academy of Science*, 109, 10233

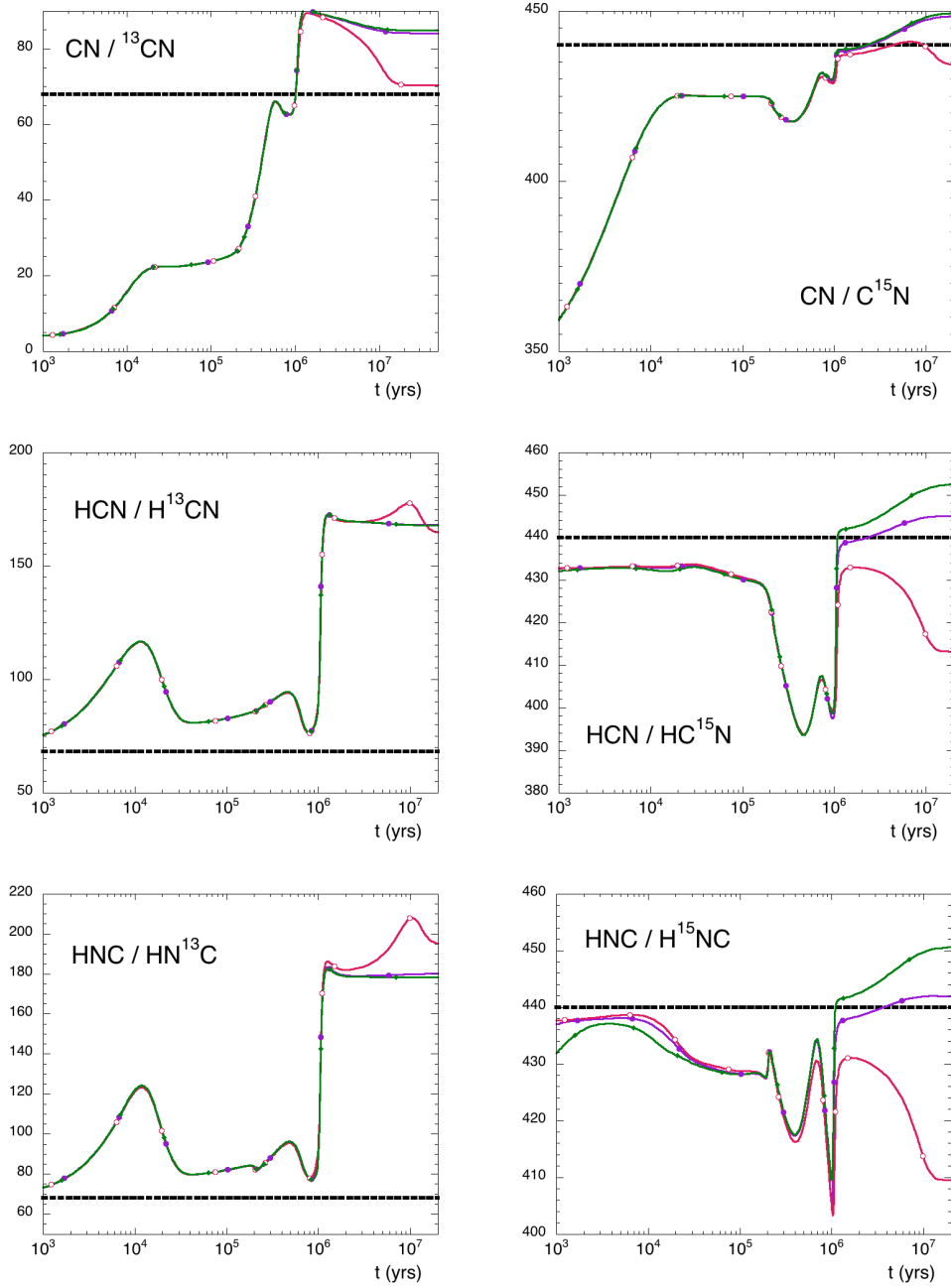


Fig. 8. Time dependence of fractionation ratios of CN, HCN, HNC in model (a) for 3 different OPR values. Black heavy dotted line: elemental ratio; green : OPR= 10^{-4} , purple : OPR = 10^{-3} , red : OPR = 10^{-2}

Daranlot, J., Hu, X., Xie, C., et al. 2013, *Physical Chemistry Chemical Physics* (Incorporating Faraday Transactions), 15, 13888
 Dislaire, V., Hily-Blant, P., Faure, A., et al. 2012, *A&A*, 537, A20
 Dore, L., Bizzocchi, L., Esposti, C. D., & Tamassia, F. 2011, *Molecular Physics*, 109, 2191
 Faure, A., Hily-Blant, P., Le Gal, R., Rist, C., & Pineau des Forêts, G. 2013, *ApJ*, 770, L2
 Flower, D. R., Pineau Des Forêts, G., & Walmsley, C. M. 2006, *A&A*, 456, 215
 Furuya, K., Aikawa, Y., Sakai, N., & Yamamoto, S. 2011, *ApJ*, 731, 38
 Gamallo, P., Martínez, R., Sayós, R., & González, M. 2010, *J. Chem. Phys.*, 132, 144304
 Georgievskii, Y. & Klippenstein, S. J. 2005, *J. Chem. Phys.*, 122, 194103
 Gerin, M., Marcelino, N., Biver, N., et al. 2009, *A&A*, 498, L9
 Gerin, M., Viala, Y., & Casoli, F. 1993, *A&A*, 268, 212

Glassgold, A. E., Huggins, P. J., & Langer, W. D. 1985, *ApJ*, 290, 615
 Grant Hill, J., Mitrushchenkov, A., Yousaf, K. E., & Peterson, K. A. 2011, *J. Chem. Phys.*, 135, 144309
 Guelachvili, G., de Villeneuve, D., Farrenq, R., Urban, W., & Verges, J. 1983, *Journal of Molecular Spectroscopy*, 98, 64
 Henry, A., Le Moal, M. F., Cardinet, P., & Valentin, A. 1978, *J. Mol. Spectrosc.*, 70, 18
 Herbst, E., Defrees, D. J., Talbi, D., Pauzat, F., & Koch, W. 1991, *J. Chem. Phys.*, 94, 7842
 Herzberg, G. 1945, *Molecular Spectra and Molecular Structure*, Vol. 2: Infrared and Raman Spectra of Polyatomic Molecules (New York: Van Nostrand), 372
 Herzberg, G. 1989, *Molecular Spectra and Molecular Structure*, Vol. 1: Spectra of Diatomic Molecules (Malabar: Krieger Publishing Company)
 Hily-Blant, P., Bonal, L., Faure, A., & Quirico, E. 2013a, *Icarus*, 223, 582

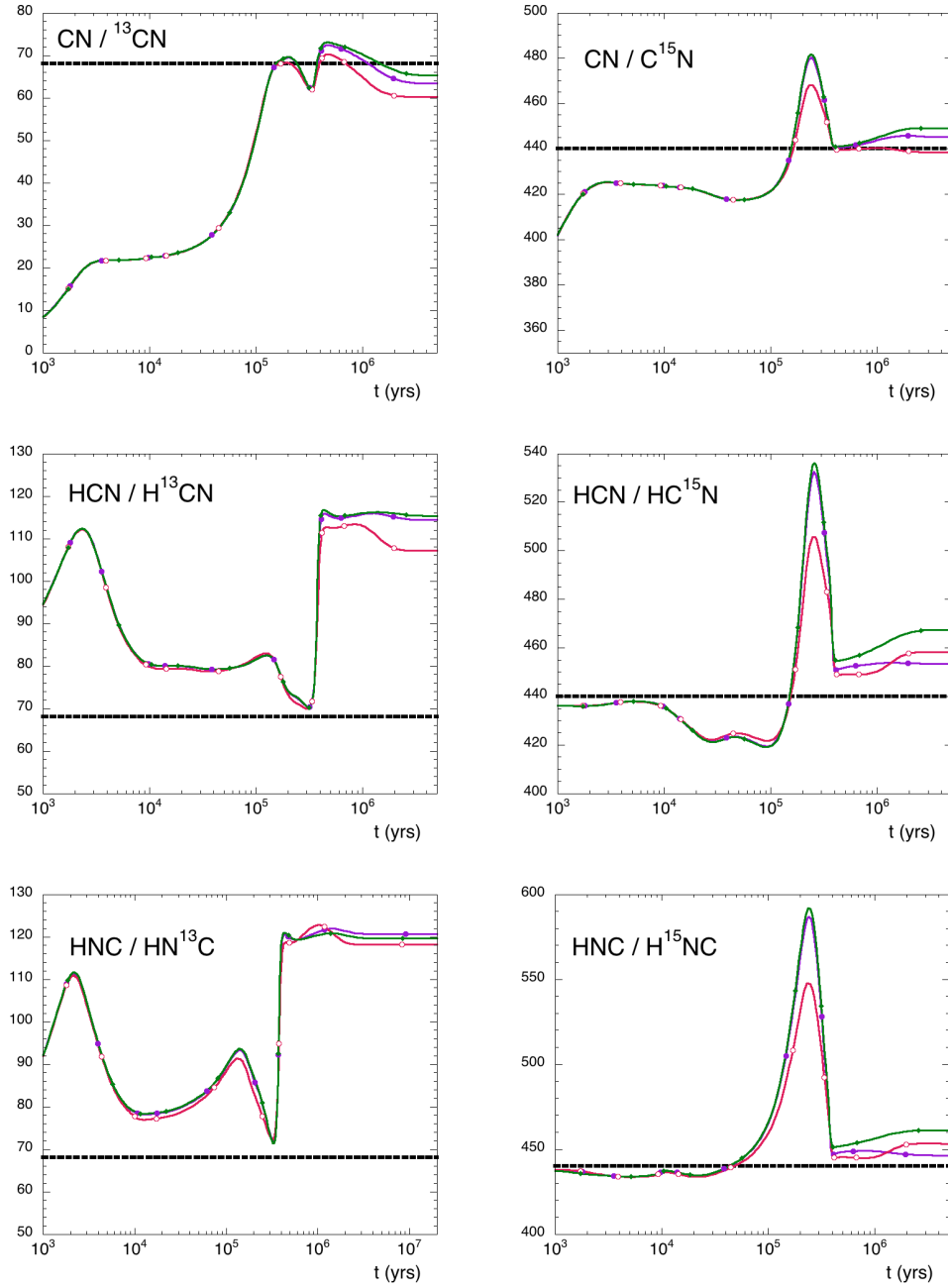


Fig. 9. Time dependence of fractionation ratios of CN, HCN, HNC in model (b) for 3 different OPR values. Black heavy dotted line: elemental ratio; green : OPR= 10^{-4} , purple : OPR = 10^{-3} , red : OPR = 10^{-2}

Hily-Blant, P., Pineau des Forêts, G., Faure, A., Le Gal, R., & Padovani, M. 2013b, A&A, 557, A65
Hirano, N. & Liu, F.-c. 2014, ApJ, 789, 50
Huang, X., Schwenke, D. W., & Lee, T. J. 2011, J. Chem. Phys., 134, 044321
Huang, X., Valeev, E. F., & Lee, T. J. 2010, J. Chem. Phys., 133, 244108
Ikeda, M., Hirota, T., & Yamamoto, S. 2002, ApJ, 575, 250
Jensen, P. & Kraemer, W. P. 1988, Journal of Molecular Spectroscopy, 129, 216
Langer, W. D., Graedel, T. E., Frerking, M. A., & Armentrout, P. B. 1984, ApJ, 277, 581
Langer, W. D. & Penzias, A. A. 1990, ApJL, 357, 477
Le Bourlot, J. 1991, A&A, 242, 235
Le Bourlot, J., Pineau Des Forêts, G., Roueff, E., & Flower, D. R. 1993, A&A, 267, 233
Le Gal, R., Hily-Blant, P., Faure, A., et al. 2014, A&A, 562, A83

Le Picard, S. D. & Canosa, A. a. 1998, J. Chem. Soc. Faraday Transactions, 94, 2889
Le Roy, R. J., Huang, Y., & Jary, C. 2006, J. Chem. Phys., 125, 164310
Lique, F., Daniel, F., Pagani, L., & Feautrier, N. 2015, MNRAS, 446, 1245
Lis, D. C., Wootten, A., Gerin, M., & Roueff, E. 2010, ApJ, 710, L49
Liszt, H. S. 2007, A&A, 476, 291
Liszt, H. S. & Ziurys, L. M. 2012, ApJ, 747, 55
Lohr, L. L. 1998, J. Chem. Phys., 108, 8012
Loison, J.-C., Wakelam, V., & Hickson, K. M. 2014, MNRAS, 443, 398
Lucas, R. & Liszt, H. 1998, A&A, 337, 246
Ma, J., Guo, H., & Dawes, R. 2012, Physical Chemistry Chemical Physics (Incorporating Faraday Transactions), 14, 12090
Maki, A. G. & Mellau, G. C. 2001, J. Mol. Spectrosc., 206, 47

- Maki, A. G., Mellau, G. C., Klee, S., Winnewisser, M., & Quapp, W. 2000, *J. Mol. Spectrosc.*, 202, 67
- Marquette, J. B., Rebrion, C., & Rowe, B. R. 1988, *J. Chem. Phys.*, 89, 2041
- Martin, J. M. L., Taylor, P. R., & Lee, T. J. 1993, *J. Chem. Phys.*, 99, 286
- Marty, B., Chaussidon, M., Wiens, R. C., Jurewicz, A. J. G., & Burnett, D. S. 2011, *Science*, 332, 1533
- Mebel, A. M. & Kaiser, R. I. 2002, *ApJ*, 564, 787
- Mendes, M. B., Buhr, H., Berg, M. H., et al. 2012, *ApJ*, 746, L8
- Milam, S. N., Savage, C., Brewster, M. A., Ziurys, L. M., & Wyckoff, S. 2005, *ApJ*, 634, 1126
- Milligan, D. B., Fairley, D. A., Freeman, C. G., & McEwan, M. J. 2000, *International Journal of Mass Spectrometry*, 202, 351
- Mitrushchenkov, A. 2014, private communication
- Mladenović, M. & Roueff, E. 2014, *A&A*, 566, A144
- Möllmann, E., Maki, A. G., Winnewisser, M., Winnewisser, B. P., & Quapp, W. 2002, *J. Mol. Spectrosc.*, 212, 22
- Ohishi, M., Irvine, W. M., & Kaifu, N. 1992, in *IAU Symposium*, Vol. 150, *Astrochemistry of Cosmic Phenomena*, ed. P. D. Singh, 171
- Pagani, L., Roueff, E., & Lesaffre, P. 2011, *ApJ*, 739, L35
- Pillai, T., Wyrowski, F., Hatchell, J., Gibb, A. G., & Thompson, M. A. 2007, *A&A*, 467, 207
- Ram, R. S. & Bernath, P. F. 2010, *J. Mol. Spectrosc.*, 260, 115
- Ram, R. S. & Bernath, P. F. 2012, *J. Mol. Spectrosc.*, 274, 22
- Ram, R. S., Wallace, L., & Bernath, P. F. 2010, *J. Mol. Spectrosc.*, 263, 82
- Rodgers, S. D. & Charnley, S. B. 2004, *MNRAS*, 352, 600
- Rodgers, S. D. & Charnley, S. B. 2008a, *ApJ*, 689, 1448
- Rodgers, S. D. & Charnley, S. B. 2008b, *MNRAS*, 385, L48
- Roueff, E., Lis, D. C., van der Tak, F. F. S., Gerin, M., & Goldsmith, P. F. 2005, *A&A*, 438, 585
- Sakai, N., Saruwatari, O., Sakai, T., Takano, S., & Yamamoto, S. 2010, *A&A*, 512, A31
- Sakai, N., Takano, S., Sakai, T., et al. 2013, *Journal of Physical Chemistry A*, 117, 9831
- Sattelmeyer, K. 2004, *Chemical Physics Letters*, 383, 266
- Savage, C., Apponi, A. J., Ziurys, L. M., & Wyckoff, S. 2002, *ApJ*, 578, 211
- Smith, D. & Adams, N. G. 1980, *ApJ*, 242, 424
- Taatjes, C. A. 1997, *J. Chem. Phys.*, 106, 1786
- Terzieva, R. & Herbst, E. 2000, *MNRAS*, 317, 563
- Tiné, S., Roueff, E., Falgarone, E., Gerin, M., & Pineau des Forêts, G. 2000, *A&A*, 356, 1039
- Vigren, E., Zhaunerchyk, V., Hamberg, M., et al. 2012, *ApJ*, 757, 34
- Visser, R., van Dishoeck, E. F., & Black, J. H. 2009, *A&A*, 503, 323
- Wakelam, V., Smith, I. W. M., Loison, J.-C., et al. 2013, *ArXiv e-prints*
- Wampfler, S. F., Jorgensen, J. K., Bizzarro, M., & Bisschop, S. E. 2014, *ArXiv e-prints*
- Wang, Q., Ding, Y.-h., & Sun, C.-c. 2005, *Chem Phys Chem*, 6, 431
- Wang, Q., Ding, Y.-h., & Sun, C.-c. 2006, *Chem Phys Chem*, 7, 710
- Watson, W. D., Anicich, V. G., & Huntress, Jr., W. T. 1976, *ApJ*, 205, L165
- Wirström, E. S., Charnley, S. B., Cordiner, M. A., & Milam, S. N. 2012, *ApJ*, 757, L11
- Zachwieja, M. 1995, *Journal of Molecular Spectroscopy*, 170, 285
- Zachwieja, M. 1997, *Journal of Molecular Spectroscopy*, 182, 18
- Zachwieja, M., Szajna, W., & Hakalla, R. 2012, *Journal of Molecular Spectroscopy*, 275, 53
- Zhang, X.-N., Shi, D.-H., Sun, J.-F., & Zhu, Z.-L. 2011, *Chinese Physics B*, 20, 043105
- Zhao, Y. & Truhlar, D. G. 2008, *Theor. Chem. Acc.*, 120, 215
- Zymak, I., Hejduk, M., Mulin, D., et al. 2013, *ApJ*, 768, 86

Table 1. Isotopic exchange reactions.

label / comment	Reaction	k_f^* ($\text{cm}^3 \text{s}^{-1}$)	$f(B, M)^*$	ΔE^* (K)
(1) A	$\text{N}^{15}\text{N} + \text{N}_2\text{H}^+ \rightleftharpoons \text{N}^{15}\text{NH}^+ + \text{N}_2$	2.3×10^{-10}	0.5	10.3
(2) A	$\text{N}^{15}\text{N} + \text{N}_2\text{H}^+ \rightleftharpoons {}^{15}\text{NNH}^+ + \text{N}_2$	2.3×10^{-10}	0.5	2.1
(3) A	$\text{N}^{15}\text{N} + {}^{15}\text{NNH}^+ \rightleftharpoons \text{N}^{15}\text{NH}^+ + \text{N}^{15}\text{N}$	4.6×10^{-10}	1	8.1
(4) B	${}^{15}\text{N}^+ + \text{N}_2 \rightleftharpoons {}^{14}\text{N}^+ + \text{N}^{15}\text{N}$	$4.8 \times 10^{-10} \times \frac{2}{2+\exp(-28.3/T)}$	2	28.3
(5) C	${}^{15}\text{N} + \text{CNC}^+ \rightleftharpoons \text{C}^{15}\text{NC}^+ + {}^{14}\text{N}$	$3.8 \times 10^{-12} \times (\frac{T}{300})^{-1}$	1	38.1
(6) D	${}^{15}\text{N}^+ + {}^{14}\text{NO} \rightleftharpoons {}^{14}\text{N}^+ + {}^{15}\text{NO}$	no react	-	24.3
(7) barrier	${}^{15}\text{N} + \text{N}_2\text{H}^+ \rightleftharpoons {}^{14}\text{N} + \text{N}^{15}\text{NH}^+$	no react	-	38.5
(8) barrier	${}^{15}\text{N} + \text{N}_2\text{H}^+ \rightleftharpoons {}^{14}\text{N} + {}^{15}\text{NNH}^+$	no react	-	30.4
(9) barrier	${}^{15}\text{NNH}^+ + \text{H} \rightleftharpoons \text{H} + \text{N}^{15}\text{NH}^+$	no react	-	8.1
(10) barrier	${}^{15}\text{N} + \text{HCNH}^+ \rightleftharpoons {}^{14}\text{N} + \text{HC}^{15}\text{NH}^+$	no react	-	37.1
(11) D	${}^{15}\text{N} + \text{CN} \rightleftharpoons {}^{14}\text{N} + \text{C}^{15}\text{N}$	upper limit : $2.0 \times 10^{-10} \times (T/300)^{1/6} \times \frac{1}{1+\exp(-22.9/T)}$	1	22.9
(12) B	${}^{15}\text{N} + \text{C}_2\text{N} \rightleftharpoons {}^{14}\text{N} + \text{C}_2{}^{15}\text{N}$	$1.6 \times 10^{-10} \times (T/300)^{1/6} \times \frac{1}{1+\exp(-26.7/T)}$	1	26.7
(13) D	${}^{15}\text{N} + {}^{14}\text{NO} \rightleftharpoons {}^{14}\text{N} + {}^{15}\text{NO}$	-	-	24.3
(14) B	${}^{13}\text{C}^+ + \text{CO} \rightleftharpoons {}^{12}\text{C}^+ + {}^{13}\text{CO}$	$6.6 \times 10^{-10} \times (T/300)^{-0.45} \times \exp(-6.5/T) \times \frac{1}{1+\exp(-34.7/T)}$	1	34.7
(15) A	${}^{13}\text{CO} + \text{HCO}^+ \rightleftharpoons \text{CO} + \text{H}^{13}\text{CO}^+$	$2.6 \times 10^{-10} \times (T/300)^{-0.4}$	1	17.4
(16) B	${}^{13}\text{C}^+ + \text{CN} \rightleftharpoons {}^{12}\text{C}^+ + {}^{13}\text{CN}$	$3.82 \times 10^{-9} \times (T/300)^{-0.4} \times \frac{1}{1+\exp(-31.1/T)}$	1	31.1
(17) B	${}^{13}\text{C} + \text{CN} \rightleftharpoons {}^{12}\text{C} + {}^{13}\text{CN}$	$3.0 \times 10^{-10} \times \frac{1}{1+\exp(-31.1/T)}$	1	31.1
(18) C	${}^{13}\text{C} + \text{HCN} \rightleftharpoons {}^{12}\text{C} + \text{H}^{13}\text{CN}$	no react	-	48.4
(19) B	${}^{13}\text{C} + \text{C}_2 \rightleftharpoons {}^{12}\text{C} + {}^{13}\text{CC}$	$3.0 \times 10^{-10} \times \frac{2}{2+\exp(-26.4/T)}$	2	26.4
(19) barrier	${}^{13}\text{CH} + \text{CO} \rightleftharpoons {}^{13}\text{CO} + \text{CH}$	no react	-	28.6

* k_f is the forward reaction rate coefficient. The reverse reaction rate coefficient, k_r , is obtained by $k_r = \frac{k_f}{f(B,M)} \exp(-\Delta E/T)$.

Table 2. Reaction rate coefficients of $\text{N}^+ + \text{H}_2$ and isotopic variants.

Reaction	k ($\text{cm}^3 \text{s}^{-1}$)	Comment
${}^{14}\text{N}^+ + p\text{-H}_2 \rightarrow \text{NH}^+ + \text{H}$	$8.35 \times 10^{-10} \times \exp(-168.5/T)$	Dislaire et al. 2012
${}^{14}\text{N}^+ + o\text{-H}_2 \rightarrow \text{NH}^+ + \text{H}$	$4.2 \times 10^{-10} \times (T/300)^{-0.17} \times \exp(-44.5/T)$	Dislaire et al. 2012
${}^{15}\text{N}^+ + p\text{-H}_2 \rightarrow {}^{15}\text{NH}^+ + \text{H}$	$8.35 \times 10^{-10} \times \exp(-164.3/T)$	see text
${}^{15}\text{N}^+ + o\text{-H}_2 \rightarrow {}^{15}\text{NH}^+ + \text{H}$	$4.2 \times 10^{-10} \times (T/300)^{-0.17} \times \exp(-39.7/T)$	see text
${}^{14}\text{N}^+ + \text{HD} \rightarrow \text{ND}^+ + \text{H}$	$3.17 \times 10^{-10} \times \exp(-16.3/T)$	Marquette et al. 1988
${}^{14}\text{N}^+ + \text{HD} \rightarrow \text{NH}^+ + \text{D}$	$3.17 \times 10^{-10} \times \exp(-594.3/T)$	see text
${}^{15}\text{N}^+ + \text{HD} \rightarrow {}^{15}\text{ND}^+ + \text{H}$	$3.17 \times 10^{-10} \times \exp(-9.3/T)$	see text
${}^{15}\text{N}^+ + \text{HD} \rightarrow {}^{15}\text{NH}^+ + \text{D}$	$3.17 \times 10^{-10} \times \exp(-589.5/T)$	see text
${}^{14}\text{N}^+ + \text{D}_2 \rightarrow \text{ND}^+ + \text{D}$	$2.37 \times 10^{-10} \times \exp(-197.9/T)$	Marquette et al. 1988
${}^{15}\text{N}^+ + \text{D}_2 \rightarrow {}^{15}\text{ND}^+ + \text{D}$	$2.37 \times 10^{-10} \times \exp(-190.9/T)$	Marquette et al. 1988

Table 3. Reaction rate coefficients of $\text{NH}_3^+ + \text{H}_2$ and isotopic variants at $T = 10\text{K}$.

Reaction			k ($\text{cm}^3 \text{s}^{-1}$)	
			present work	old value (*)
$\text{NH}_3^+ + \text{H}_2$	\rightarrow	$\text{NH}_4^+ + \text{H}$	8.2×10^{-13}	2.4×10^{-12}
$\text{NH}_3^+ + \text{HD}$	\rightarrow	$\text{NH}_4^+ + \text{D}$	8.2×10^{-13}	1.2×10^{-12}
$\text{NH}_3^+ + \text{HD}$	\rightarrow	$\text{NH}_3\text{D}^+ + \text{H}$	1.0×10^{-13}	1.2×10^{-12}
$\text{NH}_3^+ + \text{D}_2$	\rightarrow	$\text{NH}_3\text{D}^+ + \text{D}$	1.0×10^{-13}	2.4×10^{-12}
$\text{NH}_2\text{D}^+ + \text{H}_2$	\rightarrow	$\text{NH}_3\text{D}^+ + \text{H}$	8.2×10^{-13}	2.4×10^{-12}
$\text{NH}_2\text{D}^+ + \text{HD}$	\rightarrow	$\text{NH}_3\text{D}^+ + \text{D}$	8.2×10^{-13}	1.2×10^{-12}
$\text{NH}_2\text{D}^+ + \text{HD}$	\rightarrow	$\text{NH}_2\text{D}_2^+ + \text{H}$	1.0×10^{-13}	1.2×10^{-12}
$\text{NH}_2\text{D}^+ + \text{D}_2$	\rightarrow	$\text{NH}_2\text{D}_2^+ + \text{H}$	1.0×10^{-13}	2.4×10^{-12}
$\text{NHD}_2^+ + \text{H}_2$	\rightarrow	$\text{NH}_2\text{D}_2^+ + \text{H}$	8.2×10^{-13}	2.4×10^{-12}
$\text{NHD}_2^+ + \text{HD}$	\rightarrow	$\text{NH}_2\text{D}_2^+ + \text{D}$	8.2×10^{-13}	1.2×10^{-12}
$\text{NHD}_2^+ + \text{HD}$	\rightarrow	$\text{NH}_2\text{D}_3^+ + \text{H}$	1.0×10^{-13}	1.2×10^{-12}
$\text{NHD}_2^+ + \text{D}_2$	\rightarrow	$\text{NH}_2\text{D}_3^+ + \text{D}$	1.0×10^{-13}	2.4×10^{-12}
$\text{ND}_3^+ + \text{H}_2$	\rightarrow	$\text{NH}_2\text{D}_3^+ + \text{H}$	8.2×10^{-13}	2.4×10^{-12}
$\text{ND}_3^+ + \text{HD}$	\rightarrow	$\text{NH}_2\text{D}_3^+ + \text{D}$	8.2×10^{-13}	1.2×10^{-12}
$\text{ND}_3^+ + \text{HD}$	\rightarrow	$\text{ND}_4^+ + \text{H}$	1.0×10^{-13}	1.2×10^{-12}
$\text{ND}_3^+ + \text{D}_2$	\rightarrow	$\text{ND}_4^+ + \text{D}$	1.0×10^{-13}	2.4×10^{-12}

(*) Roueff et al. (2005)

Table 5. Model (a) and (b) results and observations. ss means stationary state. The value of the o/p ratio of H₂ is taken as 10⁻³.

	Model (a)		Model (b)	TMC1	L1544	B1
	t= 10 ⁶ yrs	ss	ss			
electronic fraction	1.4 × 10 ⁻⁸	2.8 × 10 ⁻⁸	1.7 × 10 ⁻⁸			
N / ¹⁵ N	440	456	455			
2 × N ₂ / ¹⁵ NN	438	431	437			
NH / ¹⁵ NH	429	428	421			
NH / ND	16	31	9			
NH ₃ / H ₂	6.7 10 ⁻⁹	1.3 10 ⁻⁹	6.0 10 ⁻⁹	2 10 ⁻⁸ (8)		
NH ₃ / ¹⁵ NH ₃	333	386	387			300 ⁺⁵⁵ ₋₄₀ (1)
NH ₂ D / H ₂	3.8 10 ⁻¹⁰	5.8 10 ⁻¹¹	3.3 10 ⁻¹⁰	4 10 ⁻¹⁰ (9)		
NH ₂ D / ¹⁵ NH ₂ D	215	276	336			230 ⁺¹⁰⁵ ₋₅₅ (1)
NH ₃ / NH ₂ D	18	22	18	50 (9)		
N ₂ H ⁺ / H ₂	4.8 10 ⁻¹⁰	1.3 10 ⁻¹⁰	2.1 10 ⁻¹⁰	5 10 ⁻¹⁰ (8)		
N ₂ H ⁺ / N ¹⁵ NH ⁺	431	430	423		1050 ^{±220} (2)	400 ⁺¹⁰⁰ ₋₆₅ (1)
N ₂ H ⁺ / ¹⁵ NNH ⁺	437	432	433		1110 ^{±240} (2)	> 600 (1)
N ₂ H ⁺ / N ₂ D ⁺	16	29	8.6	12.5 (9)		2.9 (1)
CN / H ₂	6.8 10 ⁻⁹	5.5 10 ⁻⁹	1.2 10 ⁻⁹	3 10 ⁻⁸ (8)		
CN / ¹³ CN	67	84	63			50 ⁺¹⁹ ₋₁₁ (1)
CN / C ¹⁵ N	430	449	445			240 ⁺¹³⁵ ₋₆₅ (1)
¹³ CN / C ¹⁵ N	6.4	5.3	7.0		7.5 ^{±1} (3)	
HCN / H ₂	7.4 10 ⁻⁹	5.9 10 ⁻¹⁰	5.4 10 ⁻¹⁰	2 10 ⁻⁸ (8)		
HCN / H ¹³ CN	93	168	114			30 ⁺⁷ ₋₄ (1)
HCN / HC ¹⁵ N	398	445	453			165 ⁺³⁰ ₋₂₀ (1)
H ¹³ CN / HC ¹⁵ N	4.3	2.6	4.0	2 - 4.5 (5)		5.5 ± 1 (1)
HCN / DCN	43	96	22			20 ⁺⁶ ₋₁₀ (1)
HNC / H ₂	5.6 10 ⁻⁹	7.4 10 ⁻¹⁰	8.4 10 ⁻¹⁰	2 10 ⁻⁸ (8)		
HNC / HN ¹³ C	93	180	121	54 - 72 (4)		20 ⁺⁵ ₋₄ (1)
HNC / H ¹⁵ NC	405	442	446	250 - 330 (4)		75 ⁺²⁵ ₋₁₅ (1)
HN ¹³ C / H ¹⁵ NC	2.5	1.75	3.7	4.6 ± 0.6 (4)		3.7 ± 1 (1)
HNC / DNC	23	66	16			2.9 ^{+1.1} _{-0.9} (1)
NO / H ₂	1. 10 ⁻⁷	3.1 10 ⁻⁸	4.1 10 ⁻⁸	2.7 10 ⁻⁸ (10)		
NO / ¹⁵ NO	438	451	446			
CO / H ₂	8.1 10 ⁻⁵	8.0 10 ⁻⁵	2.8 10 ⁻⁵	8 10 ⁻⁵ (8)		
CO / ¹³ CO	68	67.4	68			
CH / H ₂	1.3 10 ⁻⁹	1.7 10 ⁻⁹	1.7 10 ⁻¹⁰	2 10 ⁻⁸ (8)		
CH / ¹³ CH	74	154	71	> 71 (6)		
HCO ⁺ / H ₂	2.5 10 ⁻⁹	3.610 ⁻¹⁰	5.7 10 ⁻¹⁰	8 10 ⁻⁹ (8)		
HCO ⁺ / H ¹³ CO ⁺	56	65	56			59 (7)
HCO ⁺ / DCO ⁺	15	29	8.4	50 (9)		

References. (1) Daniel et al. (2013); (2) Bizzocchi et al. (2013); (3) Hily-Blant et al. (2013b); (4) Liszt & Ziurys (2012) ; (5) Hily-Blant et al. (2013a); (6) Sakai et al. (2013), (7) Hirano & Liu (2014) assuming CO/ C¹⁸O=500, (8) Ohishi et al. (1992), (9) Tiné et al. (2000), (10) Gerin et al. (1993).

Table 6. Dependence of the fractionation ratios on the o/p ratio of H₂ for model (a). ss means stationary state.

	OPR = 10 ⁻⁴		OPR = 10 ⁻³		OPR = 10 ⁻²	
	t= 10 ⁶ yrs	ss	t= 10 ⁶ yrs	ss	t= 10 ⁶ yrs	ss
electronic fraction	5.1 × 10 ⁻⁸	2.2 × 10 ⁻⁷	4.8 × 10 ⁻⁸	2.1 × 10 ⁻⁷	3.7 × 10 ⁻⁸	4.2 × 10 ⁻⁸
N / ¹⁵ N	440	456	440	456	440	452
2 × N ₂ / ¹⁵ NN	438	430	438	431	438	437
NH / ¹⁵ NH	431	429	429	428	426	418
NH / ND	16	31	16	31	18	23
NH ₃ / ¹⁵ NH ₃	345	409	333	386	374	395
NH ₂ D / ¹⁵ NH ₂ D	206	267	215	276	265	303
NH ₃ / NH ₂ D	8	14	17	22	43	63
N ₂ H ⁺ / N ¹⁵ NH ⁺	431	429	431	430	429	421
N ₂ H ⁺ / ¹⁵ NNH ⁺	437	432	437	432	436	433
N ₂ H ⁺ / N ₂ D ⁺	16	30	16	29	17	21
CN / ¹³ CN	67	85	67	84	67	70
CN / C ¹⁵ N	432	449	430	449	429	434
HCN / H ¹³ CN	92	168	93	168	93	165
HCN / HC ¹⁵ N	401	453	398	445	400	413
HCN / DCN	44	95	43	96	40	55
HNC / HN ¹³ C	91	178	93	180	97	195
HNC / H ¹⁵ NC	410	451	405	442	405	410
HNC / DNC	23	66	23	66	22	32
HCO ⁺ / H ¹³ CO ⁺	57	66	56	65	54	55
HCO ⁺ / DCO ⁺	15	30	15	29	16	19

Appendix A: Exchange reactions

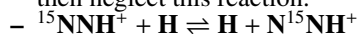
We discuss below the reactions displayed in Table 1.

- $\text{N}^{15}\text{N} + \text{N}_2\text{H}^+ \rightleftharpoons \text{N}^{15}\text{NH}^+ + \text{N}_2$
 $\text{N}^{15}\text{N} + \text{N}_2\text{H}^+ \rightleftharpoons {}^{15}\text{NNH}^+ + \text{N}_2$
 These reactions have been studied experimentally by Adams & Smith (1981) at 80 K without differentiating between N^{15}NH^+ and ${}^{15}\text{NNH}^+$. The total rate is $4.6 \times 10^{-10} \text{ cm}^3 \text{ s}^{-1}$. We thus take half this value for the forward reaction rate constant considering the symmetry factor and we assume no barrier for these rapid reactions.
 We also introduce the $\text{N}^{15}\text{N} + {}^{15}\text{NNH}^+ \rightleftharpoons \text{N}^{15}\text{NH}^+ + \text{N}^{15}\text{N}$ reaction for completeness.
- ${}^{15}\text{N}^+ + \text{N}_2 \rightleftharpoons {}^{14}\text{N}^+ + \text{N}^{15}\text{N}$
 This reaction involves adduct formation. The numerical constant is computed to reproduce the experimental value of Anicich et al. (1977) at room temperature.
- ${}^{15}\text{N} + \text{CNC}^+ \rightleftharpoons \text{C}^{15}\text{NC}^+ + {}^{14}\text{N}$
 No information is available for this reaction. The bimolecular exit channels ${}^{12}\text{C}^+ + \text{NCN}$ and C_2^+/N_2 are both endothermic by 170 and 76 kJ/mol respectively. We performed DFT calculations (at the M06-2X/cc-pVTZ level) to explore the possibility of isotopic exchange. Direct N exchange is impossible as it would require simultaneous bond formation, rearrangement and bond breaking. However, isotopic exchange could take place through adduct formation. No barrier was found in the entrance channel for NCNC^+ formation (exothermic by 167 kJ/mol). The most favorable NCNC^+ isomerization pathway is cyclic. However the position of the c-NC(N)C⁺ transition state (TS) is highly uncertain and is found to be below the entrance channel at M06-2X/cc-pVQZ level (-14 kJ/mol) but slightly above the entrance level at the RCCSD(T)-F12/aug-cc-pVTZ level (+19 kJ/mol). In any case, the TS position is close to the entrance level so that the NCNC^+ back dissociation is favored at room temperature. Isotopic exchange may however be enhanced at low temperature and may become the main exit channel. Considering a T^{-1} temperature dependence of the adduct lifetime we tentatively suggest $k_f = 3.8 \times 10^{-12} \times (T/300)^{-1} \text{ cm}^3 \text{ s}^{-1}$.
- ${}^{15}\text{N}^+ + {}^{14}\text{NO} \rightleftharpoons {}^{14}\text{N}^+ + {}^{15}\text{NO}$
 Terzieva & Herbst (2000) estimated the value of this rate coefficient from the difference between the Langevin rate and the other measured exothermic reactions reported below.

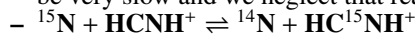
${}^{15}\text{N}^+ + {}^{14}\text{NO} \rightarrow {}^{15}\text{N} + \text{NO}^+ (k_1)$	$\Delta H_r = -509 \text{ kJ/mol}$
$\rightarrow {}^{15}\text{NN}^+ + \text{O} (k_2)$	$\Delta H_r = -213 \text{ kJ/mol}$
$\rightarrow \text{N}^{15}\text{N} + \text{O}^+$	$\Delta H_r = -402 \text{ kJ/mol}$
$\rightarrow {}^{14}\text{N}^+ + {}^{15}\text{NO}$	$\Delta H_r = -0.2 \text{ kJ/mol}$

$k_1 = 5.0 \times 10^{-10} \text{ cm}^3 \text{ s}^{-1}$ and $k_2 = 5.0 \times 10^{-11} \text{ cm}^3 \text{ s}^{-1}$. No data are available for the other two reactions. We find a barrier for NON^+ adduct formation (261 kJ/mol at the M06-2X/cc-pVTZ level) and neglect this exchange reaction.
- ${}^{15}\text{N} + \text{N}_2\text{H}^+ \rightleftharpoons {}^{14}\text{N} + \text{N}^{15}\text{NH}^+ / {}^{15}\text{NNH}^+$
 No information is available for these reactions, which were reported as crucial by Rodgers & Charnley (2008b). We performed DFT calculations (at the M06-2X/cc-pVTZ level) which showed that isotopic exchange through the addition elimination mechanism is impossible as the NN(H)N^+ and NNNH^+ ions are metastable, respectively 73 and 332 kJ/mole above the ${}^{14}\text{N} + \text{N}_2\text{H}^+$ energy. Figure A.1 displays the various possibilities. In addition, direct nitrogen exchange through $\text{NN(H)}\dots\text{N}^+ \rightarrow \text{N}\dots\text{N(H)N}^+$ presents a barrier equal to +87 kJ/mol. We did not find any N_3H^+ config-

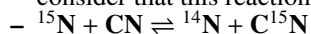
uration with an energy lower than that of the reactants. We then neglect this reaction.



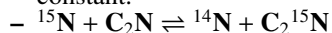
Following a similar suggestion for explaining abundance anomalies of the ${}^{13}\text{C}$ species of CCH (Sakai et al. 2010), we consider the above reaction for which no information is available. We performed various DFT calculations at the M06-2X/cc-pVTZ level. The HNNH^+ ion is 109 kJ/mole more stable than $\text{H} + \text{N}_2\text{H}^+$ but the addition reaction shows a barrier of +12 kJ/mole. The intramolecular isomerization ${}^{15}\text{NNH}^+ \rightarrow \text{N}^{15}\text{NH}^+$ displays also a barrier of +172 kJ/mole. Then direct isomerization through tunneling is expected to be very slow and we neglect that reaction ².



This reaction was also suggested by Terzieva & Herbst (2000) despite the lack of any relevant information. We performed DFT calculations to explore the possibility of isotopic exchange as shown in Figure A.2. Direct N exchange is found to be impossible as it requires simultaneous bond formation, rearrangement and bond breaking so that isotopic exchange involves adduct formation. Attack by atomic nitrogen on either side of the HCNH^+ molecular ion leads to a metastable system through high energy transition states. We did not consider transition states leading to N addition on the C=N bond of HCNH^+ nor did we examine N insertion into the N-H or C-H bonds, as all these pathways lead to species located above the reagent energy level. We did not find any CN_2H_2^+ species lying below the reagent energy level and we consider that this reaction cannot take place.



The $\text{N}(^4\text{S}_u) + \text{CN}(^2\Sigma^+)$ reaction leads to ${}^{3,5}\Sigma^-$ surfaces in $\text{C}_{\infty v}$ symmetry and ${}^{3,5}\text{A}''$ surfaces in Cs symmetry. The quintuplet surface is repulsive at the MRCI+Q/aug-cc-pVTZ level and the ${}^5\text{NCN}$ intermediate is above the $\text{N} + \text{CN}$ level. Considering only the triplet surface, the only barrierless reaction is attack on the carbon atom leading to the ground state ${}^3\text{NCN}$ intermediate (Daranlot et al. 2012; Ma et al. 2012). The main exit channel is $\text{C} + \text{N}_2$ after isomerization of the NCN intermediate through a tight TS and then back dissociation may be important and isotope exchange possible. In the nominal model we neglect this reaction but some tests have been performed to estimate its potential role. The upper limit of the isotope exchange rate constant is equal to the capture rate constant minus the $\text{N} + \text{CN} \rightarrow \text{C} + \text{N}_2$ rate constant. That value is notably smaller than the capture one at low temperature. We thus propose the upper limit value of $2.0 \times 10^{-10} \times (T/300)^{1/6} \frac{1}{1+\exp(-22.9/T)} \text{ cm}^3 \text{ s}^{-1}$ for the forward rate constant.



The $\text{N}(^4\text{S}) + \text{C}_2\text{N}(^2\Pi)$ reaction leads to ${}^{3,5}\Pi$ surfaces in $\text{C}_{\infty v}$ symmetry and ${}^{3,5}\text{A}' + {}^{3,5}\text{A}''$ surfaces in Cs symmetry. Figure A.3 displays the positions of the state energies linked to $\text{N} + \text{C}_2\text{N}$ which are calculated at the MRCI+Q/aug-cc-pVTZ level (10 e- in 10 OM with the geometry fully optimized at the CASCCF level or 14 e- in 14 OM for the CASCCF and 14e- in 12 OM for the MRCI calculation with non relaxed geometry). The triplet surface pathway leads to a NCCN adduct in a triplet state, corresponding to an excited state of the very stable NCCN linear molecule, located -393 kJ/mol below the $\text{N}(^4\text{S}) + \text{C}_2\text{N}(^2\Pi)$ level. No barrier is present in the entrance valley so that this NCCN adduct very likely leads to CN (in

² we note in addition that N_2H^+ formation from $\text{N}_2 + \text{H}_3^+$ is exothermic by only 72 kJ/mole, so that any ${}^{15}\text{NNH}^+$ produced will not isomerize into N^{15}NH^+ and vice versa.

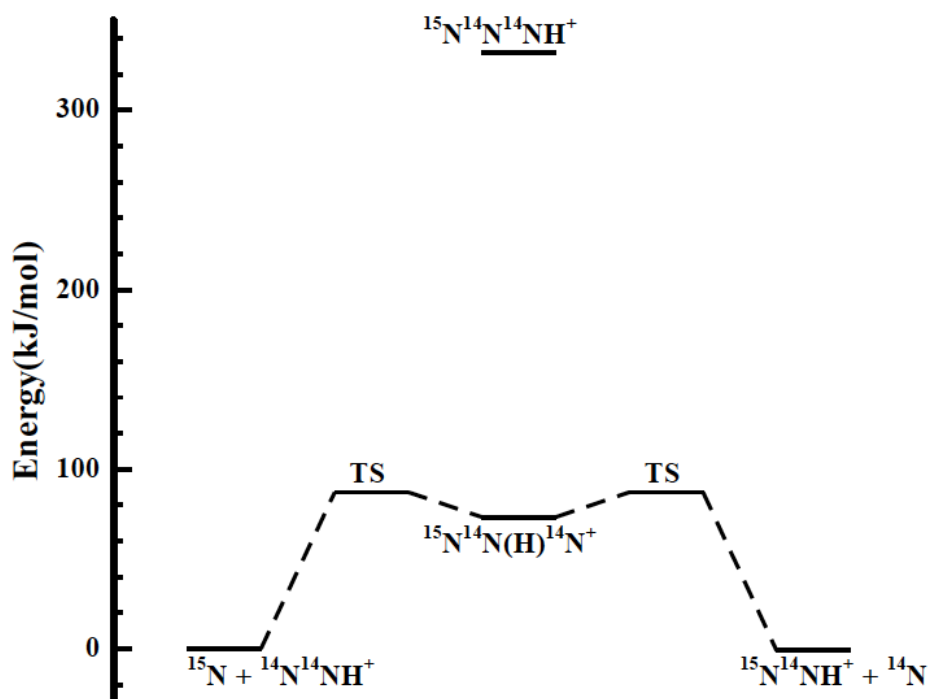


Fig. A.1. Energy diagram of the NNNH⁺ system.

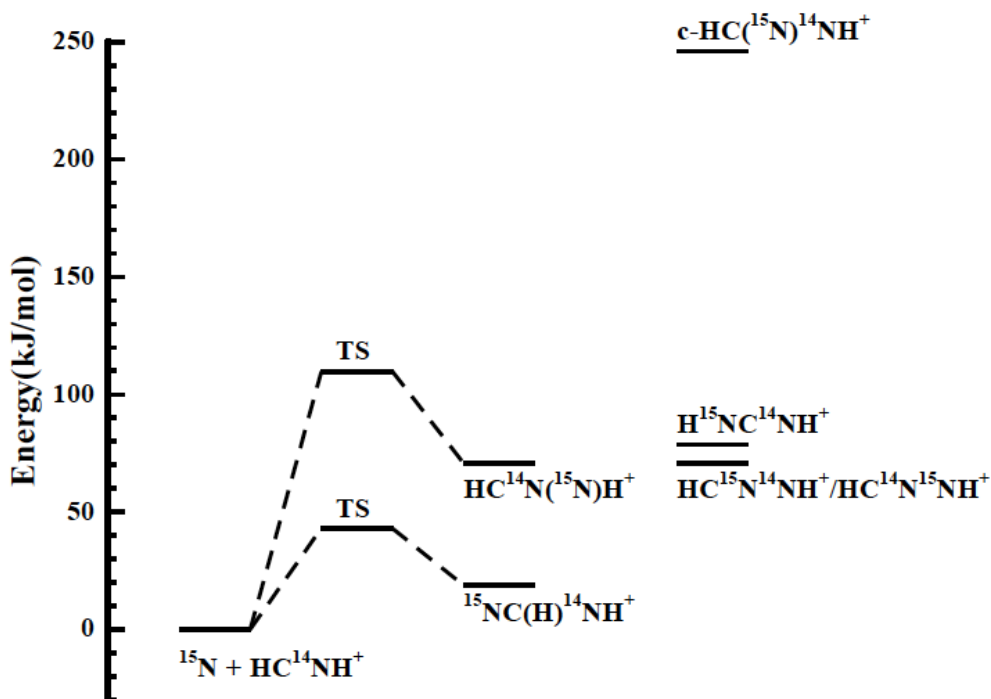


Fig. A.2. Energy diagram of the HCNH⁺ system.

a doublet state) + CN (in a doublet state) products. The occurrence of a small exit barrier cannot be excluded but its energy should be much lower than that of the $^{14}\text{N} + \text{C}_2^{15}\text{N}$ entrance channel. Triplet surfaces thus cannot lead to isotopic exchanges. However the quintuplet surface deserves specific

attention as the $\text{NCCN}(^5\Sigma^+)$ adduct is found at an energy of -183 kJ/mol below that of $\text{N}(^4\text{S}) + \text{C}_2\text{N}(^2\Pi)$ level (at the MRCI+Q, RCCSD(T) and DFT level of calculations). However, no exothermic bimolecular exit channel is available on this quintuplet surface. We thus conclude that the quintuplet

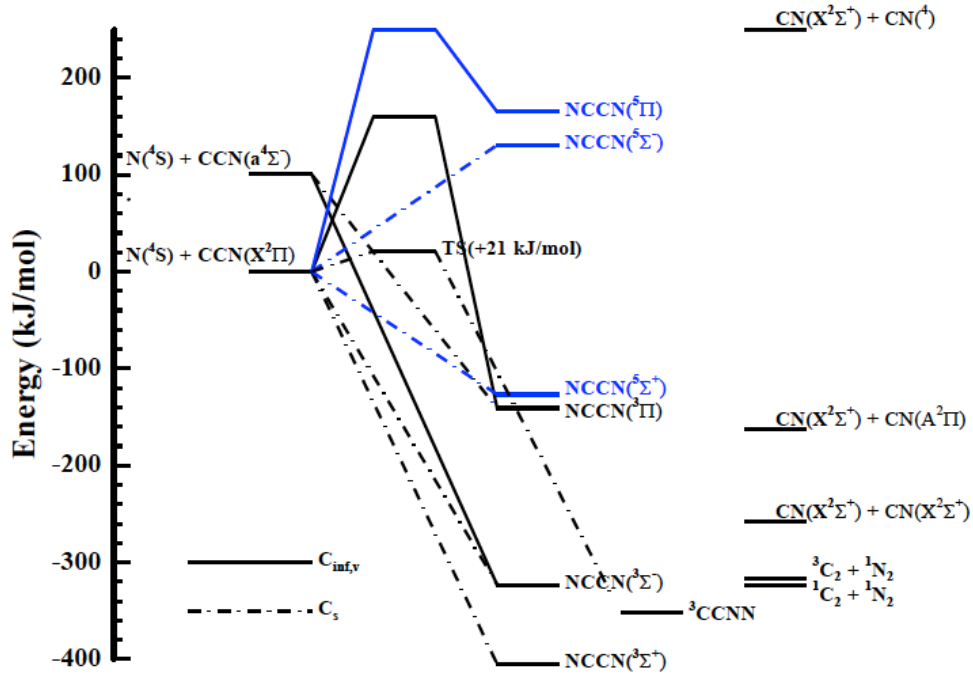
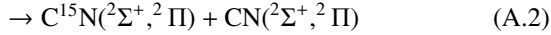
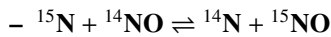


Fig. A.3. Energy diagram of the CCNN system.

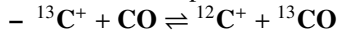
surface could lead to isotopic exchange and consider finally the two following possibilities for this reaction involving the very reactive C_2N radical (Wang et al. 2005, 2006), i.e. the triplet channel :



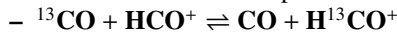
and the quintuplet channel :



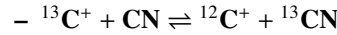
There is a barrier for NON adduct formation. The isotope exchange rate is calculated to be very low (Gamallo et al. 2010) as the main exit channel is $N_2 + O$. Moreover the quintuplet surfaces are repulsive. We neglect this reaction.



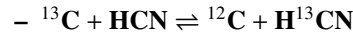
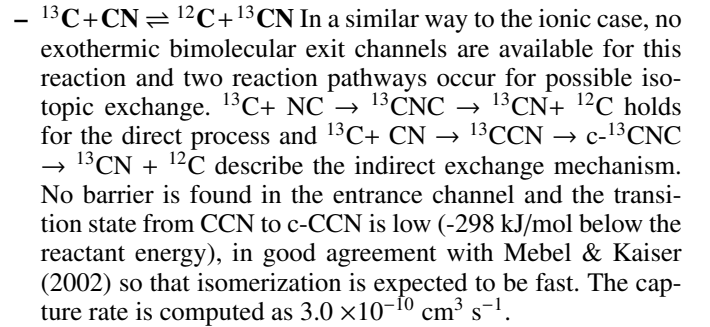
This reaction was first mentioned by Watson et al. (1976) and has been experimentally studied in detail by Smith & Adams (1980) in the 80-500 K temperature range. Their data can be fitted (Liszt 2007). We introduce a new formula allowing us to describe the full temperature range with a single formula.



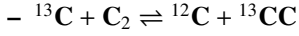
This reaction has also been studied experimentally by Smith & Adams (1980). The exothermicity of the reaction has been reported to be 9 K by Langer et al. (1984) from theoretical studies whereas Smith & Adams (1980) proposed a value of 12 ± 5 K. However, a later study by Lohr (1998) leads to a value of 17.4 K. Mladenović & Roueff (2014) have reconsidered this reaction and have confirmed the value of Lohr (1998). We include this exothermicity value in the present work. Experimental points are fitted through a power law as given in Table 1.



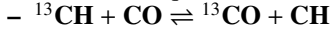
There are no bimolecular exit channels for this reaction and two different pathways lead to isotopic exchange. In a direct reaction, $^{13}C^+ + NC \rightarrow ^{13}CNC^+ \rightarrow ^{13}CN + ^{12}C^+$ whereas the indirect pathway involves $^{13}C^+ + CN \rightarrow ^{13}CCN^+ \rightarrow ^{13}CN + ^{12}C^+$. There is no barrier in the entrance valley for both cases at the M06-2X/cc-pVTZ level. Moreover, the cyclic transition state from CCN^+ and CNC^+ is located at -436 kJ/mol below the reactant energy, leading to fast isomerization. The corresponding capture rate constant is $3.82 \times 10^{-9} \times (T/300)^{-0.40}$.



There are no exothermic bimolecular exit channels for this reaction and there is no barrier for HCNC formation but isotopic exchange requires isomerization through a TS located close to the reactant level, involving a TS located at -16 kJ/mol at the M06-2X/cc-pVQZ level but +34 kJ/mol at the RCCSD(T)-F12-aug-cc-pVQZ level. Calculation of the rate constant for exchange is complex and similar to the $^{15}N + CNC^+$ case. In the nominal model we neglect this reaction. We estimate nevertheless an upper limit for the rate constant by using a $1/T$ temperature dependence and assuming that the isotopic exchange rate constant balances the back dissociation at very low temperature (3K).



There are no exothermic product channels for this reaction and there is very likely to be no barrier. The capture rate constant is equal to $3.0 \times 10^{-10} \text{ cm}^3 \text{ s}^{-1}$.



This reaction could be an additional possibility to enhance ${}^{13}\text{CO}$ as no barrier has been found in the entrance valley (Le Picard & Canosa 1998). The high pressure $\text{CH} + \text{CO} \rightarrow \text{HCCO}$ association reaction rate constant is equal to $3 \times 10^{-11} \times (T/300)^{-0.9}$ between 53 and 294 K. The exchange rate has been measured to be $\sim \times 10^{-12}$ (Taates 1997) at room temperature. This value represents 1% of the association reaction rate constant at high pressure, which is explained by a transition state localized at 6kJ/mole above the reactants energy as computed at the M06-2X/cc-pVTZ level, in good agreement with Sattelmeyer (2004). We do not include this reaction in our models given the high TS which should make this exchange process negligible at low temperature.

Table 1. Atomic Masses in amu. from NIST

Atom	Mass
H	1.007825032 07
D	2.014 101 777 8
N	14.003074004
${}^{15}\text{N}$	15.000108 898
C	12.00
${}^{13}\text{C}$	13.003354 838
O	15.994 914 619 6
${}^{18}\text{O}$	17.999 161 0
e	0.00054858

Table 2. Spectroscopic constants of diatomic molecules in cm^{-1} and differences of ZPE with respect to the main isotopologue.

Molecule	Ref	ω_e	$\omega_e x_e$	ZPE	$\Delta(\text{ZPE})$ (K)
N_2	[1]	2358.53	14.30	1175.7	-
N^{15}N	[1]	2319.01	13.83	1156.05	28.3
${}^{15}\text{N}_2$	[1]	2278.80	13.35	1136.06	57.0
NH	[2]	3282.2	78.3	1621.5	-
${}^{15}\text{NH}$	<i>computed</i>	3274.9	77.95	1617.9	5.2
ND	[3]	2399.0	42.0	1189.5	621.6
${}^{15}\text{ND}$	<i>computed</i>	2389.0	41.6	1183.6	630
NH^+	[4]	3047.58	72.19	1505.7	-
${}^{15}\text{NH}^+$	[4]	3040.77	71.87	1502.4	4.8
ND^+	[4]	2226.93	38.55	1103.8	578
${}^{15}\text{ND}^+$	<i>computed</i>	2217.60	38.23	1099.2	585
CN	[5]	2068.68	13.12	1031.1	-
${}^{13}\text{CN}$	[6]	2025.25	12.57	1009.5	31.1
C^{15}N	[7]	2036.70	12.70	1015.2	22.9
${}^{14}\text{NO}$	[8]	1904.11	14.08	948.5	-
${}^{15}\text{NO}$	[9]	1870.1	13.585	931.7	24.3
C_2	[10]	1853.5	12.755	923.98	-
${}^{13}\text{CC}$	[10]	1817.3	12.1	905.61	26.4
CO	[11]	2169.8	13.3	1081.6	-
${}^{13}\text{CO}$	[11]	2121.4	12.7	1057.5	34.7
CH	[12]	2860.75	64.44	1414.3	-
${}^{13}\text{CH}$	[13]	2852.15	64.04	1410.1	6.0
CD	[14]	2101.05	34.7	1042.1	535.5

[1] Le Roy et al. 2006, [2] Ram & Bernath 2010, [3] Dore et al. 2011, [4] Colin 1989, [5] Ram et al. 2010, [6] Ram & Bernath 2012, [7] Colin & Bernath 2012, [8] Henry et al. 1978, [9] Danielak et al. 1997, [10] Zhang et al. 2011, [11] Guelachvili et al. 1983, [12] Zachwieja 1995, [13] Zachwieja 1997, [14] Zachwieja et al. 2012

Appendix B: ZPE values

We revisit the ZPE values in light of several recent studies. We recall in Table 1 the atomic masses of various isotopes which may be used to derive spectroscopic constants of isotopic molecules, as found in basic molecular spectroscopy textbooks (Herzberg 1945, 1989). We only refer to the first order expansion terms for the purpose of computing ZPEs.

Appendix B.0.1: Diatomic Molecules

For diatomic molecules, energy levels are expressed as a Dunham expansion or equivalently as a sum of harmonic + anharmonicity correction factors. The following expression is obtained for the ZPE, corresponding to $v = 0$.

$$\text{ZPE} = \frac{1}{2}Y_{10} + \frac{1}{4}Y_{20} = \frac{1}{2}\omega_0 - \frac{1}{4}\omega_e x_e \quad (\text{B.1})$$

ω_0 is the harmonic contribution of the vibrational frequency and $\omega_e x_e$ represents the anharmonic contribution. The reduced mass μ dependence of ω_0 and $\omega_e x_e$ are $1/\sqrt{\mu}$ and $1/\mu$ respectively. The label *computed* in Table 2 indicates the use of this property to compute the spectroscopic constants, in the absence of other information.

Appendix B.0.2: Polyatomic molecules

For polyatomic molecules, the following expression extends the diatomic formulae where the different vibrational degrees of freedom are included:

$$G_0 = \sum_i \omega_i \frac{d_i}{2} + \sum_i \sum_j x_{ij} \frac{d_i}{2} \frac{d_j}{2} \quad (\text{B.2})$$

ω_i refers to the harmonic frequencies, d_i is the corresponding degeneracy and x_{ij} stands for the anharmonic terms. The sum is performed over the number of vibrational modes. In the case of polyatomic linear molecules, the number of vibrational modes is $3N-5$ whereas it is $3N-6$ in the general case where N is the number of nuclei in the molecule.

Table 3. Spectroscopic constants of triatomic molecules in cm^{-1} and differences of ZPE with respect to the main isotopologue.

Molecule symmetry	Ref	ω_1 Σ^+	ω_2 Π	ω_3 Σ^+	ZPE	$\Delta(\text{ZPE})$ (K)
HCN	[1]	3443.1	727.0	2127.4	3512.25	-
H ¹³ CN	[1]	3424.0	720.6	2093.0	3478.6	48.4
HC ¹⁵ N	[1]	3441.7	725.9	2094.0	3493.75	26.6
H ¹³ C ¹⁵ N	[1]	3422.6	719.5	2058.6	3460.1	75.0
DCN	[2]	2702.5	579.7	1952.3	2883.9	904.1
CCN	[3]	1967.2	322.2	1058.3	1794.20	-
¹³ CCN	[3]				1778.19	23.0
C ¹³ CN	[3]				1761.11	47.6
CC ¹⁵ N	[3]				1775.65	26.7
HNC	[4]	3819.9	463.8	2064.3	3369.9	-
HN ¹³ C	[4]	-	463.5	-		
H ¹⁵ NC	[4]	-	461.5	-		
N ₂ H ⁺	[5]	3398.6	695.5	2297.7	3508.6	-
¹⁵ NNH ⁺	[5]	3396.5	694.4	2259.3	3487.5	30.4
N ¹⁵ NH ⁺	[5]	3382.4	690.7	2268.7	3481.8	38.5
¹⁵ N ₂ H ⁺	[5]	3380.7	699.6	2229.3	3460.4	69.3
N ₂ D ⁺	[5]	2719.8	550.4	2065.9	2916.2	852
N ¹⁵ ND ⁺	[5]	2680.4	544.4	2058.8	2888.4	40.0
¹⁵ NND ⁺	[5]	2703.8	549.0	2041.0	2895.2	30.2
CNC ⁺	[6]	1335	165	2040	1852.5	-
C ¹⁵ NC ⁺	[6]	1334	161	1997	1826	38.1
HCO ⁺	[7], [9]	3229.6	832.5	2195.8	3524.60	-
H ¹³ CO ⁺	[8],[9]	3206.1	824.9	2160.6	3488.24	52.3
DCO ⁺	[7],[9]	2645.9	666.5	1928.0	2944.22	835.1

[1] Maki et al. (2000), [2] Möllmann et al. 2002, [3] Grant Hill et al. 2011; Mitrushchenkov 2014, [4] Maki & Mellau 2001, [5] Huang et al. 2010, [6] Jensen & Kraemer 1988, [7] Martin et al. 1993, [8] private communication by T. Lee, based on second-order vibrational perturbation theory using a quartic force field determined at the CCSD(T)/cc-pVTZ level of electronic structure theory, as in [7], [9] ZPEs are from Mladenović & Roueff (2014).

Table 4. Spectroscopic constants of tetratomic nitrogen molecules in cm^{-1} and differences of ZPE with respect to the main isotopologue.

Molecule symmetry	Ref	ω_1 Σ	ω_2 Σ	ω_3 Σ	ω_4 Π	ω_5 Π	ZPE	$\Delta(\text{ZPE})$ (K)
HCNH ⁺	[1]	3484.2	3187.3	2159.9	804.8	649.4	5987.3	-
H ¹³ CNH ⁺	[1]	3479.5	3170.1	2126.1	799.8	647.4	5952.0	50.8
HC ¹⁵ NH ⁺	[2]	3469.3	3187.1	2133.3	804.7	645.1	5961.5	37.1
HCND ⁺	[1]	3221.9	2681.1	2025.9	794.3	513.1	5364.2	896.5
DCNH ⁺	[1]	3474.0	2601.0	1934.8	664.7	622.8	5388.0	862.3
Molecule symmetry	Ref	ω_1 A_1	ω_2 A_1	ω_3 E	ω_4 E		ZPE	$\Delta(\text{ZPE})$ (K)
NH ₃	[3]	3336.1	932.4	3443.6	1626.3		7429.2	-
¹⁵ NH ₃	[3]	3333.3	928.5	3435.1	1623.2		7413.0	23.3

[1] Brites & Jutier 2012, [2] Brites, private communication, [3] Huang et al. 2011